

arXiv:0808.1315v1 [astro-ph] 8 Aug 2008

VERY LARGE TELESCOPE  
**ASTRONOMICAL MULTI-BEAM RECOMBINER**  
**AMBER**

**February 2008 ATF run report<sup>1</sup>**

Doc. No VLT-TRE-AMB-15830-7120

Issue 1.2

Date : 16/04/2008

	Prepared	Approved	Released
Function	AMBER Task Force <sup>1</sup>	Principal Investigator	Project Manager
Name	A. Chelli, G. Duvert, P. Kern, F. Malbet (chair)	Romain Petrov	Pierre Antonelli
Signature			

<sup>1</sup> With the support of F. Rantakyö (ESO)

OCA/UNSA LAOG MPIfR/OAA	<b>VLT / AMBER</b>	Doc. No VLT-TRE-AMB-15830-7120
	February 2008 ATF run report <sup>1</sup>	Issue : 1.2
		Date : 16/04/2008
		Page : ii

## Change record

Issue	Date	Update sections	Reason / remarks
0.1-0.5	14/02/2008- 21/03/2008	all	drafts
1.0	24/03/2008	all	first released version
1.1	14/04/2008	E.1	Added new material related to spectral displacement
1.2	16/04/2008	A.3	Added recommendation, etc. on full-frame P2VM characterisation

OCA/UNSA LAOG MPIfR/OAA	VLT / AMBER	Doc. No VLT-TRE-AMB-15830-7120
	February 2008 ATF run report <sup>1</sup>	Issue : 1.2
		Date : 16/04/2008
		Page : iii

# Contents

<b>CONTENTS</b>	<b>iv</b>
<b>ACRONYMS AND ABBREVIATIONS</b>	<b>v</b>
<b>1 Introduction</b>	<b>1</b>
1.1 Scope of the report . . . . .	1
1.2 Outline of the report . . . . .	1
1.3 Documents . . . . .	1
1.3.1 Applicable documents . . . . .	1
1.3.2 Reference documents . . . . .	1
<b>2 Data processing analysis</b>	<b>1</b>
<b>3 Hardware system analysis</b>	<b>2</b>
3.1 Detector quality . . . . .	2
3.2 Optical alignment . . . . .	2
3.2.1 Focus and tip-tilt alignment of the detector and the spectrograph . . . . .	2
3.2.2 Alignment of the pupil and adjustment of the focalizer . . . . .	2
3.2.3 Optical ghosts . . . . .	2
3.3 Optical stability . . . . .	2
3.3.1 Stability of output beams . . . . .	3
3.3.2 Optical path stability . . . . .	3
3.3.3 CAU stability . . . . .	3
3.3.4 Recommendations . . . . .	3
3.4 Spectral dispersion . . . . .	3
3.4.1 Grating position . . . . .	3
3.4.2 Spectral shifts . . . . .	4
3.4.3 Spectral calibration of the low resolution JHK mode . . . . .	4
3.5 Internal calibration source . . . . .	4
<b>4 Performance limitations</b>	<b>4</b>
4.1 Closure phase corruption . . . . .	4
4.2 Phase beating in differential phase . . . . .	4
4.3 Fluctuation of the contrast . . . . .	5
4.4 AMBER performance on sky . . . . .	6
<b>5 Recommendations</b>	<b>7</b>
<b>A Data processing analysis</b>	<b>9</b>
A.1 Characterization of the AMBER P2VM . . . . .	9
A.2 An improved data reduction software . . . . .	9
A.3 On the P2VM spatial extension . . . . .	12
<b>B Optical alignment</b>	<b>14</b>
B.1 Adjustment of the DET/SPG focus . . . . .	14
B.2 Pupil alignment and focaliser adjustment . . . . .	14
<b>C Characterization of ghosts</b>	<b>18</b>
C.1 Mismatch of photometric calibration . . . . .	18
C.2 Investigating P2VM calibration files prior to Feb 2008 . . . . .	18
C.3 Ghosts measured during ATF . . . . .	22
C.4 Conclusions and recommendations . . . . .	23

OCA/UNSA LAOG MPIfR/OAA	<b>VLT / AMBER</b>	Doc. No VLT-TRE-AMB-15830-7120
	February 2008 ATF run report <sup>1</sup>	Issue : 1.2
		Date : 16/04/2008
		Page : iv

<b>D Optical stability</b>	<b>24</b>
D.1 Output beams . . . . .	24
D.1.1 Medium term stability survey during the ATF operation . . . . .	24
D.1.2 Sensitivity to vibrations . . . . .	24
D.2 P2VM stability . . . . .	25
D.3 CAU stability . . . . .	25
D.4 Conclusion: on alignment requirements and health checking . . . . .	25
<b>E Analysis of the spectral resolution</b>	<b>31</b>
E.1 Spectral shifts between photometric and interferometric channels . . . . .	31
E.2 Spectral calibration in low resolution JHK mode . . . . .	33
E.3 Calibration of visibility losses due to temporal coherence . . . . .	34
<b>F Internal light sources and effect on closure phases</b>	<b>36</b>
F.1 Analysis of internal sources . . . . .	36
F.2 Effect on closure phase calibration . . . . .	36
<b>G AMBER polarizers</b>	<b>38</b>
G.1 Polarizers current design . . . . .	38
G.2 Influence of polarizers on the AMBER observables . . . . .	39
G.3 Where to put the new polarizers? . . . . .	41
<b>H Fabry-Pérot interferometer principle</b>	<b>42</b>
<b>I Piezos controlling differential OPDs</b>	<b>43</b>
<b>J Influence of injection into the fibers</b>	<b>44</b>
<b>K Observing calibrators without polarizers</b>	<b>45</b>
<b>L Log book of the ATF run</b>	<b>50</b>

OCA/UNSA LAOG MPIfR/OAA	<b>VLT / AMBER</b>	Doc. No VLT-TRE-AMB-15830-7120
	February 2008 ATF run report <sup>1</sup>	Issue : 1.2
		Date : 16/04/2008
		Page : v

## Acronyms and abbreviations

AD	Applicable document
ADC	Atmospheric dispersion compensation
AGN	Active galactic Nucleus
AIT	Assembly, Integration and Tests
AMBER	Astronomical Multi-BEam Recombiner
AO	Adaptive optics
AT	Auxiliary telescope (1.8m)
ATF	AMBER task force
BCD	Beam commuting device
COM	Commissioning run
DDL	Differential delay line
DIT	Detector integration time
DL	Delay line
EGP	Extrasolar Giant Planet
ETC	Exposure Time Calculator
FT	Fringe tracking
ITF	Interferometry Task Force
HR	High resolution (12000)
LR	Low resolution (35)
MR	Medium resolution (1000)
OB	Observation block
OPD	Optical path difference
P2VM	Pixel to visibility matrix
PDR	Preliminary Design Review
PPRS	Paranal Problem Report System
PRIMA	Phase reference imaging and micro-arcsecond astrometry
REF	Reference documents
SNR	Signal-to-noise ratio
SOB	Sequence of Observation Blocks
SOW	Statement of Work
SS	Star separator
TBC	To be confirmed
TBD	To be defined
TEC	Technical run
UT	Unit telescope (8m)
VIMA	VLTI Main Array (array of 4 UTs)
VISA	VLTI Sub Array (array of ATs)
VLT	Very Large Telescope
VLTI	Very Large Telescope Interferometer
YSO	Young Stellar Object
ZOPD	Zero optical path difference

OCA/UNSA LAOG MPIfR/OAA	VLT / AMBER	Doc. No VLT-TRE-AMB-15830-7120
	February 2008 ATF run report <sup>1</sup>	Issue : 1.2
		Date : 16/04/2008
		Page : 1 / 51

## 1 Introduction

### 1.1 Scope of the report

The AMBER Task Force described in document [RD 1] the objectives, its methodology and its plan to investigate the various AMBER issues which prevent the instrument to fulfill its initial specifications and therefore its original science program.

The objectives of the February run was mainly to bring AMBER (see AMB-ATF-001 memo) into contractual specifications the accuracy of the absolute visibility, of the differential and of the closure phase through a fundamental analysis of the instrument status and limitations.

### 1.2 Outline of the report

Before the run, a new implementation of the AMBER software by A. Chelli and G.Duvert has been designed. This new and more accurate software using the same philosophy as the `amdlib` v2.1<sup>2</sup> is described in Sect. 2. The first days of the run were dedicated to the alignment of AMBER and characterization of its behavior. Many issues were tackled and the results are reported in Sect. 3. Then we focused our attention on the main objective of our run: the performances limitations due to phase beating and to the lack of absolute calibration reported in Sect. 4. We end our report with the AMBER Task Force recommendations given in Sect. 5.

*Note: we tried to keep the main part of the report as concise as possible and we moved the details in annexes.*

### 1.3 Documents

#### 1.3.1 Applicable documents

Code	Title	Number
AD 1	AMBER Technical Specifications	VLT-SPE-ESO-15830-2074 issue 1.0 dated 20.04.2000

#### 1.3.2 Reference documents

Code	Title	Number
RD 1	AMBER Task Force: Objectives, Methodology, Plan	VLT-PLA-AMB-15830-7003 issue 1.0 dated 13/12/2008
RD 2	ATF detailed plan for Feb'08 run	AMB-ATF-001 issue 1.5 dated 28/01/2008
RD 3	AMBER data processing in the Image space	AMB-IGR-018 issue 1.0 dated 26/10/2000
RD 4	Report of the AMBER detector intervention from September 10 to 19, 2007	AMB-DET-007 issue 1.0 dated 28/09/2007
RD 5	OPM Warm Optics Design Report	VLT-TRE-AMB-15830-1001 issue 2.2 dated 28/05/2001
RD 6	OPM Warm Optics Test Report	VLT-TRE-AMB-15830-1010 issue 1.0 dated 10/10/2003

## 2 Data processing analysis

In order to contribute to a better understanding of the AMBER/VLTI system, we have developed a software to model the experimental P2VM, and our own data reduction software to have a full control of each step of the data reduction process which was not possible using the actual `amdlib` package written in C language. The detailed implementation is described in appendix A.

<sup>2</sup>`amdlib` v2.1 is the last public release of the AMBER data reduction software.

OCA/UNSA LAOG MPIfR/OAA	<b>VLT / AMBER</b>	Doc. No VLT-TRE-AMB-15830-7120
	February 2008 ATF run report <sup>1</sup>	Issue : 1.2
		Date : 16/04/2008
		Page : 2 / 51

Although we have not been able to test all modes of AMBER with the ATF software, we think that it brings significant improvements with a visible impact on the final sensitivity limit. The P2VM modeling allows to characterize fully the instrument performance and should be used as a health check test. To achieve the best possible performance with the P2VM scheme, we propose that the P2VM should be characterized over all the camera, not on the 32 pixels wide strips of the observation (see app. A.3).

### 3 Hardware system analysis

The first days of the run were dedicated to the alignment of AMBER and characterization of its behavior. We summarize below the various issues which we have been facing.

#### 3.1 Detector quality

The result of the work on the detector quality in September is found excellent. No more detector fringes, very low number of bad pixels. The reader is referred to the report on the AMBER detector intervention in September 2007, by U.Beckmann (see [RD4] for details).

#### 3.2 Optical alignment

##### 3.2.1 Focus and tip-tilt alignment of the detector and the spectrograph

After the intervention on SPG, and the complete cooling of the whole SPG/DET dewar, a proper alignment was performed between the detector (DET) and the spectrograph (SPG) to provide a well focused image of the input slit on the detector and to align it along a the pixel line. The full alignment procedure is provided in appendix B and will be inserted in the suitable AMBER documentation.

##### 3.2.2 Alignment of the pupil and adjustment of the focalizer

All pupils were properly adjusted in order to match the cold pupil mask and the beam position launched by all the H and K dichroics and the J mirrors. It corresponds to optimized values of the flux while inserting the cold masks (3T\_K and 3T\_JHK). After the operation, all the translation stages of the mirror or dichroic support were no longer at the limits of their possible strokes. During the same operation we properly aligned the last parabolic mirror (focalizer). The warm optics adjustment improved significantly the image quality. All 0<sup>th</sup> order images in J, H, and K are smaller than  $25 \times 2.5$  pixels and the image angle is  $180^\circ \pm_{-2}^{+0.5}$  (see appendix B for details).

We recommend that this focalizing mirror must not be used for beam adjustment on the spectrograph slit, but the periscope mirrors instead.

##### 3.2.3 Optical ghosts

Appendix C shows that in the data processing a major problem came from a mismatch of the photometric calibration. We analyzed the historical data acquired prior to the Feb 2008 ATF run as well as new data taken during the run.

We found that there is a residual ghost at a 6% level in the interferometric channel. The remaining ghost is most probably due to internal reflexion inside the spectrograph dewar and it cannot be removed by any alignment of the warm optics. The effect of the ghost can be fully corrected by the software described in Sect. 2 and Appendix A.

We recommend to implement the compensation of the interferometric ghost effects in the `amdlib` library and to identify some quality checks for the P2VM calibration.

#### 3.3 Optical stability

The stability of the instrument has been an issue for a long time. Therefore we tried to characterize this stability during the ATF run.

OCA/UNSA LAOG MPIfR/OAA	VLT / AMBER	Doc. No VLT-TRE-AMB-15830-7120
	February 2008 ATF run report <sup>1</sup>	Issue : 1.2
		Date : 16/04/2008
		Page : 3 / 51

### 3.3.1 Stability of output beams

We have taken daily the position of the beams on the detector with no spectral resolution in order to detect possible drifts. During this survey, no significant drifts were observed within a time scale of a few days. During all this period, we did not perform any adjustment of the optics located after the fiber outputs in the laboratory. Day by day survey of the beam positions and beam fluxes are reported in appendix D. Less than 10% contrast losses requires overlapping at the level of 5 pixels in X and of 0.6 pixels in Y. Figure 14 in appendix D shows that during the ATF run the beams were always within specifications. Our understanding is that the effort done by Paranal to achieve a better stability of AMBER by cutting and strengthening the optomechanical elements were fruitful.

In the same appendix D, we have reported an experiment to see if the output beams were subject to vibrations and the definitive answer is negative.

We recommend to relax the alignment requirements, in order to avoid too frequent interventions in the laboratory, and implement the strategy described in Appendix D, section D.4

### 3.3.2 Optical path stability

The OPD is not stable especially after a major adjustment (several tens of microns). Relaxation time is about 1 day also possibly due to the large CAU mirror (see below). In Sect. D.2 of appendix D, we show that 2 P2VMs taken respectively at the beginning of the night and this end displays same basic features except for the phase on one baseline.

### 3.3.3 CAU stability

It has been observed that the large parabolic mirror of the CAU present significant instabilities. After tuning operations on the AMBER table, fluctuations of the OPD are observed for hours, and stable situation is attained again after one day. These instabilities may reach up to 100 nm on 1-3 baseline. These fluctuations are directly observed under slight knocking of the mirror support (see Fig. 18), and are present each time a noise source happens on the AMBER table (BCD movements, CAU motor movements certainly, large piezo movements...). We suspect that photometric noise (due to changes in injection in the fibers) is associated with each vibration of this mirror.

### 3.3.4 Recommendations

We recommend to avoid any too frequent realignment of the output optics which appears not necessary at all. For the OPD, normally if the translation stages of the input dichroics are not used, they should reach their relaxation position. However, one could implement the P2VM calibration which allow to not depend on the actual OPD. Finally, in order to improve the calibration process, solutions to fix the large CAU parabolic mirror must be found.

## 3.4 Spectral dispersion

### 3.4.1 Grating position

The grating motor seems to behave in pre-summer 2007 conditions. It losses steps, shifting globally the images of the camera by a few pixels (less than 20) . This does not preclude operation since the camera sub-windows can in general be *positioned according to this shift*.

However the software developed in Summer 2007 years to measure the shift and recenter the images on predefined positions on the camera, results in too many calls to the rotation of the grating.

We recommend to update the OS and templates in order to avoid moving the grating more than once per configuration.

*NOTE: a recent PPRS, No. 026605 reports that the MACCON board was defective and the change of the board improved a lot the reproducibility.*



OCA/UNSA LAOG MPIfR/OAA	VLT / AMBER	Doc. No VLT-TRE-AMB-15830-7120
	February 2008 ATF run report <sup>1</sup>	Issue : 1.2
		Date : 16/04/2008
		Page : 4 / 51

### 3.4.2 Spectral shifts

The spectrograph is well-aligned. The spectral shifts between photometric channels and the interferometric ones is characterized and should not be recomputed each time (see appendix E) for details.).

The spectral shift is primarily due the combination of the position of the slit (large, narrow, etc) and of a small angle between the optical components that fold the 3 photometric beams on the camera (3 glued total-reflexion prisms). At the worst, this combination changes only by a small amount every time the spectrograph is opened.

We recommend to stop using the spectral calibration procedure and use the fixed shifts.

### 3.4.3 Spectral calibration of the low resolution JHK mode

We performed a Fourier Transform Spectrograph analysis of AMBER Low Resolution JHK spectra by moving incrementally by steps of 0.01 microns the piezos on beams 1 and 3 for each band (see appendix E). Each pixel of the Interferometric region on the camera of AMBER (32 by 60 pixels in this LR mode) is thus modulated with a period equal to the wavelength it sees. The Dispersion law is found compatible with a linear dispersion of coefficients,  $\lambda = 2.6917 - 3.2082 \cdot 10^{-2} \times i$ , with  $i$  as the pixel number.

## 3.5 Internal calibration source

For tests, the RAS (Remote Alignment Source) was replaced by a laboratory source directly connected to the K band fiber of the CAU. In this condition, while the K band dichroic of the RAS is bypassed, the modulation of the flux in all photometric channels is significantly reduced and is not detectable any more in the raw data in MR (see appendix F). LR image in JHK in this condition allows a detection for all bands

The two CAU fibers suffer from incorrect superposition, since the JH fiber seems to be moving and requires some readjustments. This misalignment lead to non-zero phase closure measurement on the CAU, with an unstable value (see below Sect. 4.1).

We recommend to remove the CAU dichroic and to use only one fiber as the one for the CAU bypassing the 2 dichroics of the calibrations sources (RAS and CAU).

## 4 Performance limitations

Our main goal for the AMBER Task Force run was to find the origin of the performance limitations of AMBER. We have performed various experiences until we found the principal origin of these limitations: the polarizers.

### 4.1 Closure phase corruption

Previous data set showed that the closure phase signal was corrupted. We realize that by shutting down the remote alignment source (RAS) JH fiber, the K spectrum becomes very different. Residual K band light the RAS JH fiber polluted the K source. Therefore the instrument was seeing a binary made by the strong K fiber and the residual K light going through the JH fiber. By shutting down the RAS light leads to a closure of  $0^\circ$  all over the K band (see Fig. 24 in appendix F).

### 4.2 Phase beating in differential phase

Is called phase beating a periodic oscillation of the phase as illustrated in the left part of Fig. 1. We did intensive tests to find the origin of the phase beating:

- **Crossing the fibers.** No improvement was found. Crossing does not change injection significantly, but adds a 7.5 mm piston. Although fringes are still visible in HR, there is no significant improvement on phase beating.
- **Removing the polarizers.** The result was quite impressive:

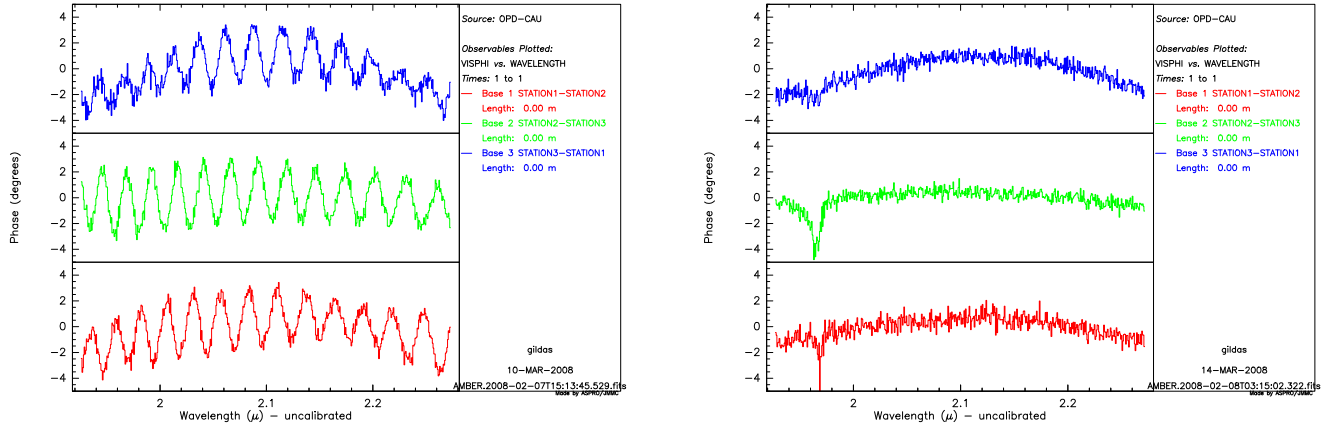


Figure 1: Differential phases measured on the internal source. Left figures were taken with the current set up using the polarizers whereas right figures were taken with the POL taken out. The feature at  $1.97\mu$  is due to a strong absorption/polarisation of the RAS dichroic

- no more fringe beating (see Fig. 1);
  - lower fringe contrast (see Fig. 27) by half which means that polarizers help to increase the contrast;
  - the flux in K is much higher and the spectrum is very different with no longer stripes;
- **One of the polarizer inserted after the fiber outputs.** The polarizer (POL3) placed at the output of the fibers close to the periscope in collimated beams, led to a much higher contrast: 0.9 0.9 0.85 for the different baselines.
  - **POL3 inserted just before the spectrograph entrance.** We put POL3 just before the spectrograph in a convergent beam. It was not successful because although there was a certain gain in contrast, it also generated a lot of unstable flux modulation.

The most probable explanation is a Fabry-Pérot effect (described in appendix H). AMBER documentation provides a description of the polarizers which is recalled in appendix G. The polarizers are made of two prisms separated by an air blade whose thickness is about 120 microns. These air blades can induce a fringe beating in a more complex way than a single Fabry-Pérot effect, because it is not the same in the different arms and leads to additional beating fluctuations both in phase and in amplitude (see for example Fig. 26).

This FP effect cannot be calibrated by the BCD because the fringe shape change too rapidly probably due to the change of the Fabry-Pérot thickness.

We recommend therefore to use other types of polarizers with no parallel optical faces and to use them in a common collimated beams after the fibers.

### 4.3 Fluctuation of the contrast

The second effect that we investigated is the origin of the fluctuation of the visibilities on sky. These fluctuations seems to be larger than the ones expected because of the atmospheric turbulence. Therefore we tried to identify the hardware on the instrument that could be at the origin of these fluctuations (see log book in appendix L).

We did several experiments:

- **Piezos shut down.** To check that the piezos were not generating any vibrations, we shut them down. This was not easy, since when plugged off the fiber head are shifted by half stroke (about 40 microns). The input dichroics had to be used to compensate for the differential OPDs. Figs. 30 and 31 illustrate that the visibility

OCA/UNSA LAOG MPIfR/OAA	<b>VLT / AMBER</b>	Doc. No VLT-TRE-AMB-15830-7120
	February 2008 ATF run report <sup>1</sup>	Issue : 1.2
		Date : 16/04/2008
		Page : 6 / 51

## Observations performed on 2008-02-14

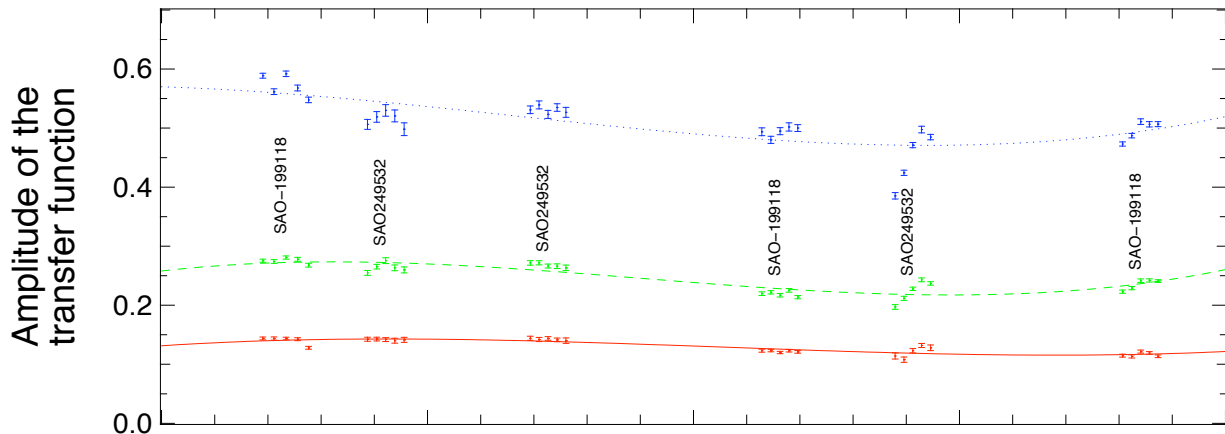


Figure 2: AMBER resulting transfer function without the polarizers.

fluctuations are still present and even reinforced due to the OPD instability (cf. Sect. 3.5): it could reach 10 to 15%...

- **Checking the beam overlap on the detector.** One possible explanation could be that due to vibrations the beam overlap is changing with time on the detector. A data set taken with no spectral resolution (see Fig. 16) showed that the beam positions in X and Y but also in flux do not change significantly with time or at a level much less than 1%.
- **Data recording with different DIT.** Using different Detector Integration Time (DIT), the fluctuations kept the same strength therefore rejecting the possibility to have fluctuations due to vibrations.
- **Using the beam commuting device (BCD).** No special effect found and also the fluctuations are not reproductive.
- **Removing the polarizers.** Data taken with the polarizers and without them (see Figs. 26 and 27 in appendix G) show clearly that the phase beating can be very important and most of all variable! The remaining variability may come from an additional effect on the internal source (see Sect. 3.3.2).
- **Injection into fibers.** The new piezo-controlled 'Iris Fast Guiding' (hereafter IFG) positioning of the AMBER entrance beams and the availability of the AT beacons were used to test whether the injection of the beam creates or increases the "phase beating" effect. No effects are detectable when the polarizer was removed. In the presence of the polarisers, however, amplitude effects are present and vary in shape with the injection. The small changes in the positioning of the beams demonstrates how sensitive the experiment is to the differential Fabry-Pérot effect induced by the polarizers.
- **CAU optical path stability.** One possibility for the fluctuations present even without the polarizers is an instability in the CAU subsystem. Monitoring the AMBER observables when touching various mechanical supports of the CAU showed that the large parabolic mirror of the CAU (see Fig. 19 in Appendix D) might be at the origin of some fluctuations. We stopped the investigation in lab and to check what would be the results on sky without using the CAU (see next section).

In conclusion, we believe that the origin of the visibility fluctuations are the results of 2 effects: the Fabry-Perot differential effect changing with time coupled to an instability of a large parabolic mirror in the alignment unit.

### 4.4 AMBER performance on sky

It is too preliminary to conclude on the overall performances of the instrument, but it seems that even with a reduced instrumental contrast, AMBER limiting magnitude is similar and even better than previously known and can measure

OCA/UNSA LAOG MPIfR/OAA	<b>VLT / AMBER</b>	Doc. No VLT-TRE-AMB-15830-7120
	<b>February 2008 ATF run report<sup>1</sup></b>	Issue : 1.2
		Date : 16/04/2008
		Page : 7 / 51

small visibilities. The closure phase and differential phases seems to be limited by fundamental (to be checked with SNR calculations) noise and no longer with systematics from the instruments.

The last night of the ATF run, we have observed repeatedly two calibrator stars in medium resolution without the polarizers together with another star of larger expected diameter. The resulting transfer function is not fully stable, but can be fitted with a polynomial of order 3. The evolution is of the order of less than 5% and can be accounted for seeing (see appendix K).

In addition differential phases on all baselines and closure phase are stable all along the night with an accuracy of  $5 \cdot 10^{-3}$  rad and 5 deg respectively.

Also AMBER has not been tested in all modes, we believe that the polarizers and the CAU mirror were the main sources of visibility fluctuations. We still have low resolution data with and with FINITO to investigate in order to assess the actual performance. However the only assessment which will be valid would be the one made with a new polarizer to get higher contrast.

## 5 Recommendations

We recommend the AMBER consortium and the ESO responsables:

- (1) to take actions as soon as possible to replace the current POL unit with a single polarizer put in the common beam before the spectrograph without Fabry-Perot effect,
- (2) to investigate the origin of the sensitivity to vibrations of the CAU parabolic mirror and fix it
- (3) to simplify the calibration light sources (RAS)
- (4) to fully characterize the instrument in its final state with a final commissioning run
- (5) to correct the AMBER observing software to minimize spectral grating movements
- (6) to update the observing software and data reduction pipeline with optimum visibility computation and quality controls.
- (7) to take the P2VM with a much larger width than the observations ( $\geq 64$  pixels channel width).

<b>OCA/UNSA LAOG MPIfR/OAA</b>	<b>VLT / AMBER</b>	Doc. No VLT-TRE-AMB-15830-7120
	February 2008 ATF run report <sup>1</sup>	Issue : 1.2
		Date : 16/04/2008
		Page : 8 / 51

## **Annexes**

OCA/UNSA LAOG MPIfR/OAA	VLT / AMBER	Doc. No VLT-TRE-AMB-15830-7120
	February 2008 ATF run report <sup>1</sup>	Issue : 1.2
		Date : 16/04/2008
		Page : 9 / 51

## A Data processing analysis

In order to contribute to a better understanding of the AMBER/VLTI system, we have developed an IDL software to model the experimental P2VM, and our own data reduction software, also written in IDL language, to have a full control of each step of the data reduction process which was not possible using the actual `amdlib` package written in C language.

### A.1 Characterization of the AMBER P2VM

The P2VM is fully described by the  $v_k$  parameters and by the carrying waves  $c_k$  and  $d_k$  (see memo AMB-IGR-018 for the definitions [RD 3], and also Tatulli et al. 2007, A&A 464, 29). The  $v_k$  parameters allow to compute the continuum in the interferometric channel from the measurements of the photometric channels. However, the presence of optical ghost (see Sect. 3.2.3) affects the  $v_k$  calculation, and the computed continuum does not strictly match anymore the true interferometric channel continuum. To solve this problem to the first order, we introduce a new way to compute the  $v_k$  parameters, which takes into account the flux in the 3 photometric channels.

The experimental P2VM is then fitted by a synthetic P2VM. The latter being perfect by construction, the output of the P2VM modelling represents the signature of the AMBER system from the calibration lamp to the scientific detector. This signature can be expressed in terms of 4 observables for each spectral channel:

- the system visibility
- the spatial frequency
- the phases of the carrying waves  $c_k$  and  $d_k$
- a continuum regularization parameter

The continuum regularization parameter is introduced to take into account an eventual residual continuum mismatch. If the  $v_k$  parameters are correctly computed, then this parameter should be close to 1, which is generally the case with the new procedure.

We present the results of the P2VM modelling for 2 sets of data. The first set of data is the P2VM of the Alpha Ara data test set obtained in Feb 2005 during SDT at medium resolution in the K band. The results are plotted in Fig. 3, for each baseline, as a function of the wavelength. At the top we see the system visibilities, with a mean value of about 0.8 beyond  $2\mu m$ . Below, we find the spatial frequencies (expressed in  $\text{pixel}^{-1}$ ) whose careful examination (at higher magnification) shows that the spectral dispersion is not constant, but is a linear function of the wavelength. Then, we see the phases of the two carrying waves whose curvatures indicate that interferometric pattern is also curved along the spectral axis. At the bottom, the phase differences between the  $c_k$  and  $d_k$  are reasonably well within the  $\pi/2$  specifications.

The second set of data is a P2VM acquired on December 29th, 2007, in low resolution mode. The results are plotted in Fig. 4. The low resolution P2VM visibility is in the range 0.5 to 0.8, with large variations from one spectral band to the other. The decrease around 1.5 and  $2\mu m$  is simply due to the superposition of two fringe systems at different spatial frequencies. Also, we may observe some structures within each band. Below, we find the 3 frequency systems and the phases of the two carrying waves. The phase discontinuities between the bands correspond to the observed shifts between the 3 fringe systems. The phase differences are plotted at the bottom.

### A.2 An improved data reduction software

The characteristics of the new data reduction software are as follows:

- the P2VM is computed as described in the previous section
- a regularization continuum parameter is applied to each interferogram. This parameter is estimated fitting the mean interferogram with 7 parameters (3 complex coherent fluxes and 1 continuum parameter)

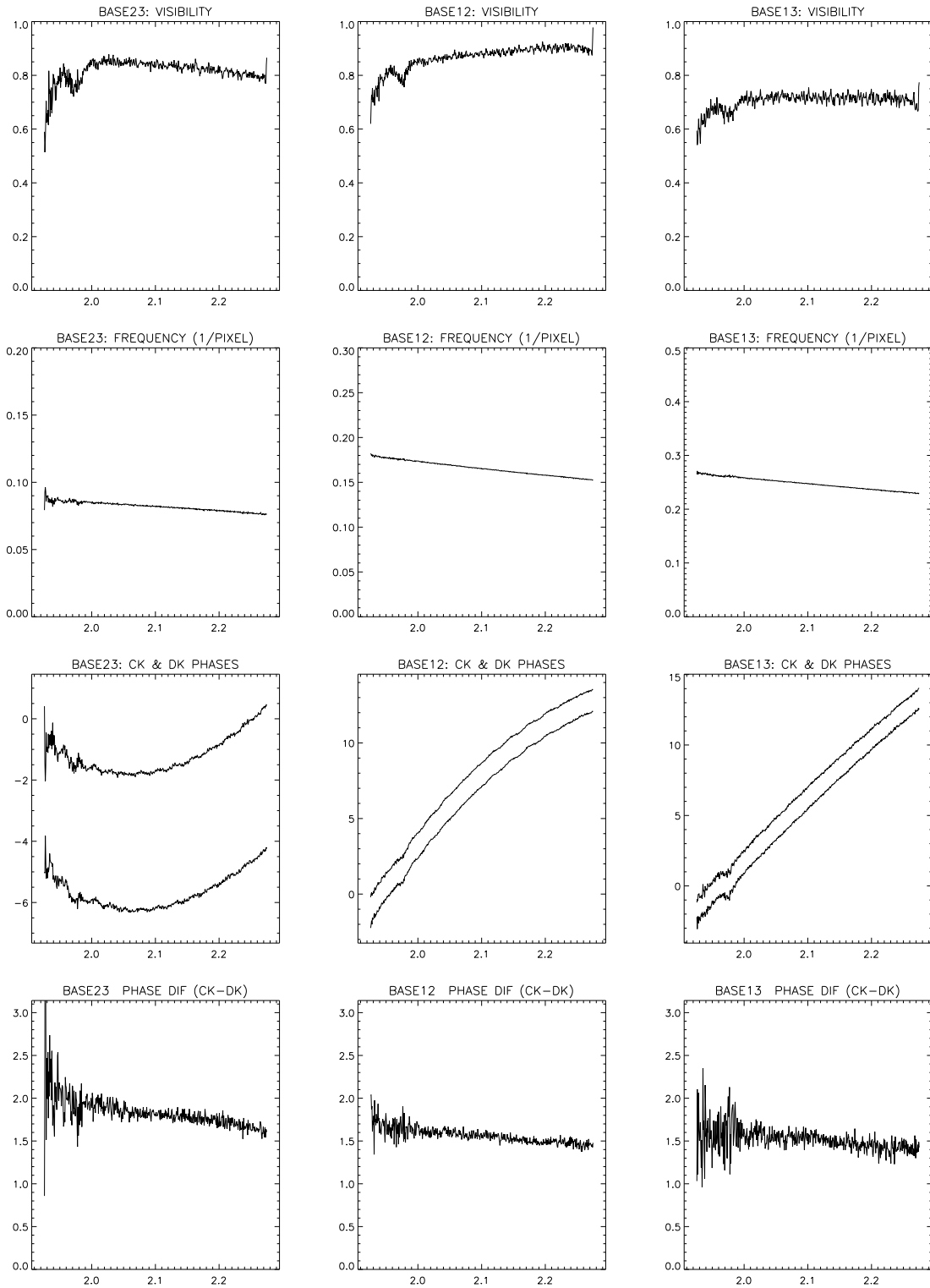


Figure 3: Characterization of the medium resolution P2VM in the K band at 3 telescopes. From top to bottom, as a function of the wavelength: P2VM visibility, frequency of the carrying waves (in  $\text{pixel}^{-1}$ ), phases of the carrying waves (in radians), phase difference between  $d_k$  and  $c_k$ . P2VM data set acquired for observations on  $\alpha$  Arae obtained in Feb 2005 during SDT.

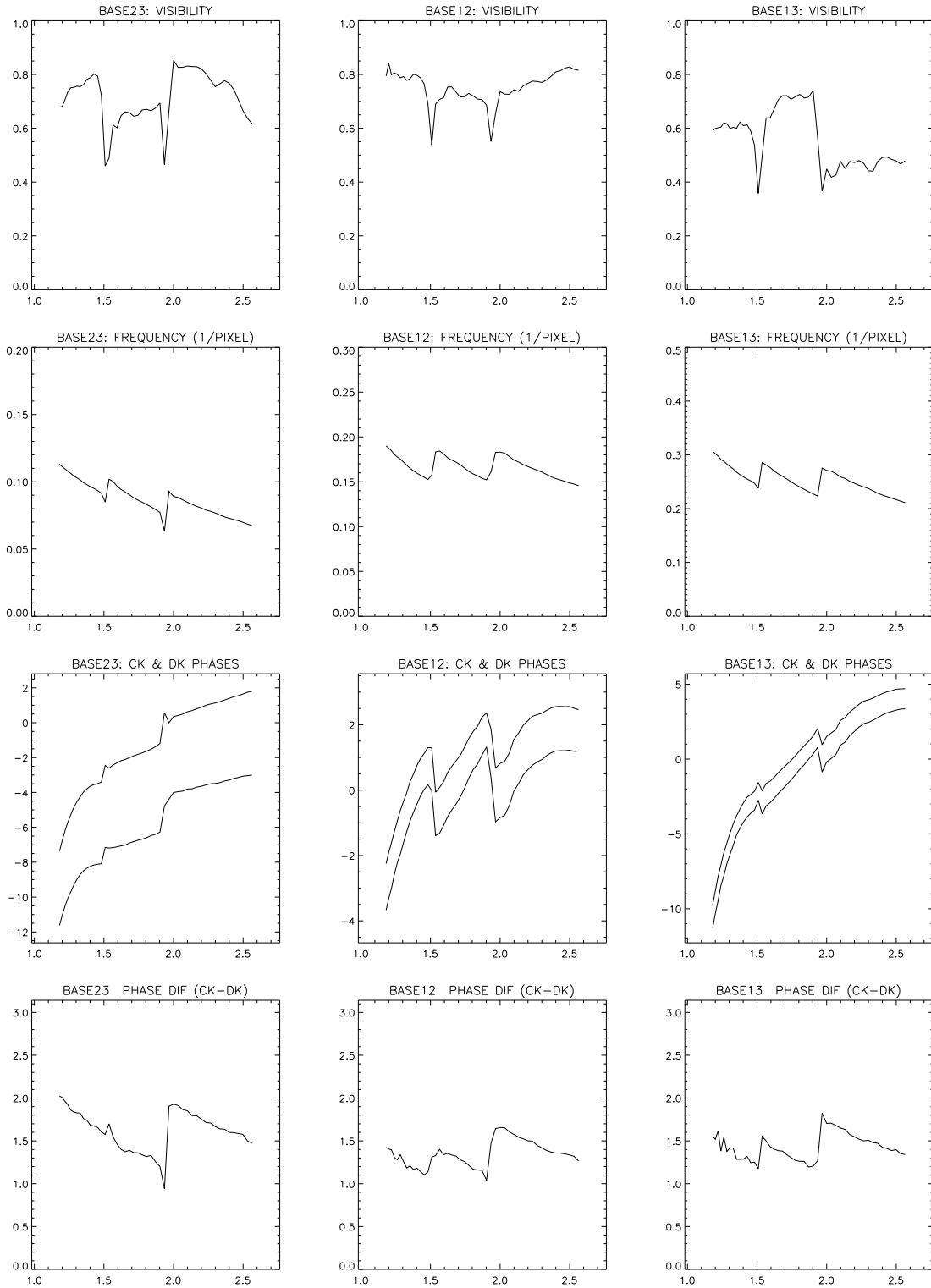


Figure 4: Characterization of the low resolution P2VM at 3 telescopes. From top to bottom, as a function of the wavelength: P2VM visibility, frequency of the carrying waves (in  $\text{pixel}^{-1}$ ), phases of the carrying wave (in radians), phase difference between  $d_k$  and  $c_k$ . P2VM data set acquired for private observations obtained in Dec 2007.



- A special attention has been given to the calculation of the covariance matrix of the measurements. The noise resulting from the detector readout noise and the background is estimated from the dark data. The covariance matrix takes into account the correlation between the measurements, and as a consequence is not diagonal. This matrix is inverted spectral line by spectral line.

This new data reduction software has been used to reduce all the data of the ATF run. The detail of the algorithm will be published elsewhere.

Figure 5 shows the relative improvement in S/N for an observation in the test dataset available with amdlib v2.1. It consists of high S/N data taken in good observing conditions in 2005, with the UTs.

The results need a few comments. This is one case where the new algorithm should not produce markedly different results, since the S/N in each frame is strong and statistics are dominated by the vibrations of UT+VLT presents at this date. We forced the spectral displacement values obtained in sect. 3.4.2 for both data reductions, since this is the good value to use, whereas the standard (pipeline) reduction would have used quite different values. The prescribed standard data reduction, in particular in this UT case where vibrations were present, calls for frame selection, however results with the new software are obtained without frame selection (hence the lower visibilities). The gain in S/N is partially due to this, and is more striking in the phase closure.

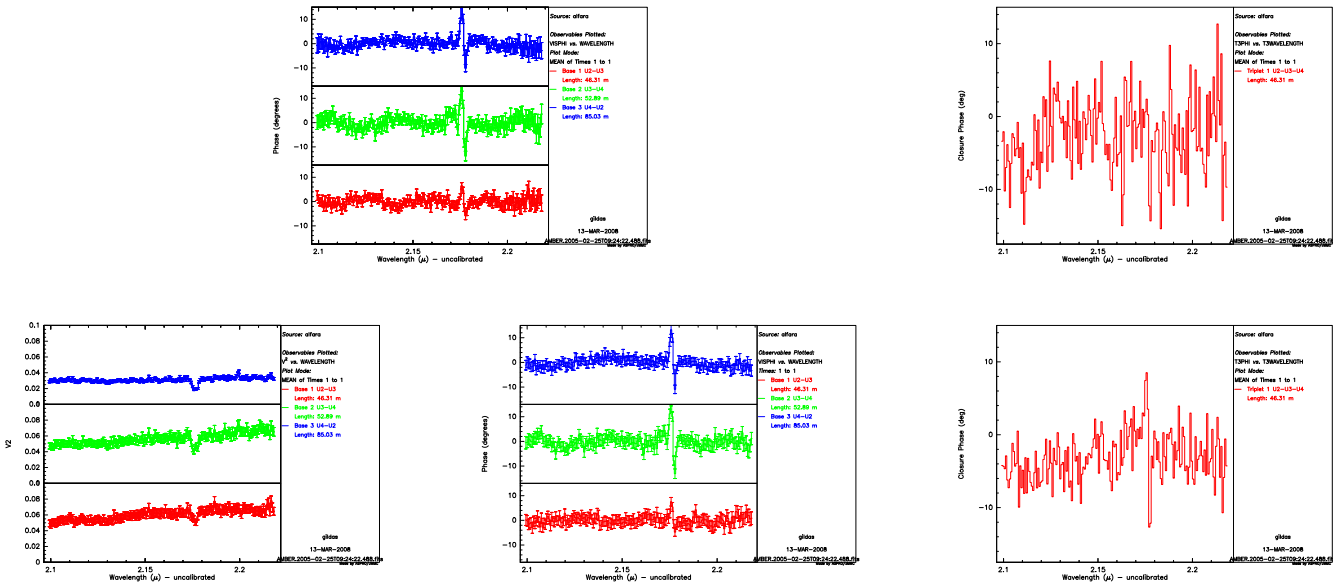


Figure 5: Comparison of noise levels on  $\alpha$  Arae data, one exposure (500 frames of 70 ms). X axis is Wavelength (microns). From left to right: Squared Visibilities, Differential Phases and Closure Phase. Top panels are amdlib v2.1 results with standard frame selection, bottom ones use ATF method, with no selection.

### A.3 On the P2VM spatial extension

The P2VM, as its name suggests, is the mean to convert pixels intensities to correlated fluxes. Its spatial extension on the camera needs not, and should not, be restricted to the 32 pixels wide strips used for the observation.

We have checked that restricting the P2VM extension to the 32 pixels is not harmful in terms of loss of information, since the 6 independent parameters of the 3 simultaneous complex correlated fluxes are more than sufficiently fitted on 32 independent pixel values (24 would suffice in theory).

However, we found that in the current AMBER setup where the characterization of  $C_k$ s and  $D_k$ s depends on the phase induced by an air blade of variable properties (temperature, humidity, repeatability of piezo), one needs the best possible determination of this phase. Errors on this phase measurement will convert into power wrongly transferred between the real and imaginary parts of the instantaneous complex coherent flux proportionally to the piston and the piston jitter.

<b>OCA/UNSA LAOG MPIfR/OAA</b>	<b>VLT / AMBER</b>	Doc. No VLT-TRE-AMB-15830-7120 Issue : 1.2
	<b>February 2008 ATF run report<sup>1</sup></b>	Date : 16/04/2008
		Page : 13 / 51

To minimize the errors in this phase measurement, one needs to measure by an integral method the phase between the  $C_k$ s and  $D_k$ s with the maximum possible spatial extension, at least 64 pixels instead of the current 32 (TBC).

OCA/UNSA LAOG MPIfR/OAA	VLT / AMBER	Doc. No VLT-TRE-AMB-15830-7120
	February 2008 ATF run report <sup>1</sup>	Issue : 1.2
		Date : 16/04/2008
		Page : 14 / 51

## B Optical alignment

### B.1 Adjustment of the DET/SPG focus

While the dewar was open for maintenances on DET and SPG, we had to adjust properly the focus and tilt of the camera with respect to the spectrograph. A first alignment done during the cooling of the spectrograph was not sufficient.

This alignment is done using the Cold Stop slit at the entrance of the spectrograph, imaged on the camera in normal cold conditions (see Fig. 6). Before starting the alignment, the two brakes of the tuning device must be released (4 screws each beneath the support). The brakes are located on the bottom of the cryostat support on each side. It is better to completely release also the two guiding spheres (3 set of large guiding screws) that allows the three rotation around a point close to the detector. The upper sphere guides the rotations around the optical axis (horizontal axis driven by the 2 vertical screws) and the tilt of the detector (around the vertical axis using the 2 horizontal screws). The lower sphere allows the tip around the horizontal axis within the plane of the detector.

The focus is performed using the long screw located beneath the support (using a key #7 (tbc)) . The focusing is monitored while the slit is imaged in the middle of the detector (0 order / cold stop / Pupil Technics) with a flat illumination (a flash light). The orientation of the slit on the detector is adjusted to be parallel to the columns of the detector.

The tip-tilt is monitored while moving the slit image from one side of the focal plane array to the other one using the movement of the grating. The slit image must be lower than 2 pixels at the center, and must be enlarged by the same amount on the two sides.

In the present case, the previous alignment, due to the lack of time after the maintenance of the grating turret, was probably done before the whole assembly was properly cooled down.

We adjusted the setting to achieved the required tuning, and achieve a 2 pixels large focusing of the cold stop.

Note: doing this measurement one can observe a duplication of the interferometric beam slit, corresponding to a parasitic image (see Fig. 6). Latter measurements showed that this ghost induce fringes in the beam 2. The translation of the ghost with respect to the interferometric beam is 2 pixels down and around 2 pixels to the left side.

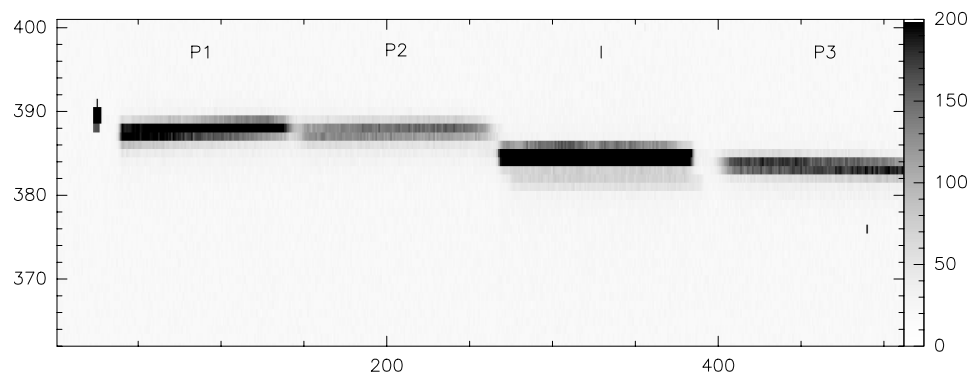


Figure 6: Image of the smaller slit (COLD stop) on the detector. Note that interferometric part of the image (third beam) is duplicated by 2 pixels down and right. One can see the ghost reported in appendix C in the interferometric channel.

### B.2 Pupil alignment and focaliser adjustment

The focaliser mirror was completely re-aligned, considering the wrong position of all of its tuning knobs and its obvious misalignment. The alignment start by putting all setting in medium position, which consist in removing all apparent angle of the parabolic mirror with respect to the optical beam. The tilt of the beam image on the camera (spectro set at zero order) can be due to the tilt of this parabolic mirror. It must be noticed that this mirror must NOT be used to adjust the position of overall beams on the SPG entrance slit. This setting must be done using the 2 translation stages of the periscope, one on each mirror that correspond to the 2 directions.

OCA/UNSA LAOG MPIfR/OAA	<b>VLT / AMBER</b>	Doc. No VLT-TRE-AMB-15830-7120
	<b>February 2008 ATF run report<sup>1</sup></b>	Issue : 1.2
		Date : 16/04/2008
		Page : 15 / 51

During this alignment we corrected pupil vigneting on the previous 45° mirror where beam 2 and 3 were obscured by its mechanical mount. To correct this vigneting it was necessary to adjust the dichroic angles (output K dichroic in this case). The correction was performed using the dichroic tip-tilt of the beam K2, and then all dichroics were adjusted with respect to the new position of the output K2 dichroic. It was performed an adjustment of the beam print on the 3TK cold pupil inside the cryostat in order to reach the higher signal. In the mean time we determine the correct position of the 3TK pupil mask (-44804 position). It was determined by a maximization of the flux in the image. At the end of the procedure:

- Image position is tuned using the angular tuning of the dichroic, and maximizing the image flux
- Pupil position is tuned using the dichroic translation and maximizing also the image flux
- Check of the image position (and adjustment with angular adjustment)
- Check of the pupil position using the Pupil imaging lens of the detector (manual knob on the detector). The pupil image through the mask is not overlapping the pupil print as seen with a wide field illumination of the spectrograph (flash light)

Doing the alignment of the focaliser we improved a lot the image quality of all the beams. For all J H and K beams the images on the camera are lower than 25x2 pixel with a mean spot angle of 179° (between 178 and 180).

All H and K pupils were then adjusted to fit the 3TK and 3TJHK pupil mask using the adjustments of the H dichroic beam splitters for H band, and the adjustments of the J mirrors for J band (tilts for image positions and translations for pupil adjustments while checking the flux level). In all cases the flux reduction while introducing the pupil mask do never exceed 5% with respect to the images without any pupil mask (see tabled values).

The optimized value for the two masks are now entered in the ICS.

- 3TK mask position: -44804,
- 3T JHK mask position: -27330

Doing the pupil adjustments, most of the translation stages acting on the OPD were released toward their medium position and no translation stages are not any more in extremal position.

The figures report the positions of the beams on the the input parabola (see Fig. 7) and on the pupil alignment mask located at the output of the Spatial Filters (see Fig. 8).

It must be mentioned that this alignment requires to proceed accurately taking into account all related parameters, using the input and output dichroic translations and the piezo actuator support.

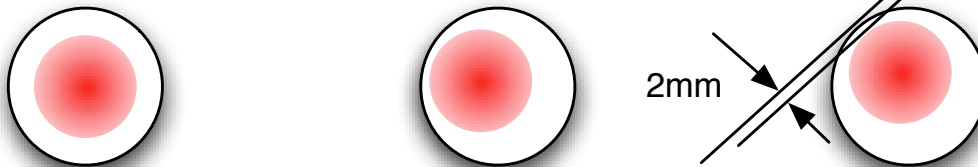
- Piezo support is an independent support, but its translation may strongly affect the beam injection, due to its poor guiding capability. Be aware that if the flux is lost in the fiber, the process is heavy to get it back.
- Input dichroic translation affect the beam position on input parabolas
- output dichroic translation affects the pupil position on pupil mask in the cryostat. It may also introduce vigneting for related beams (the beam itself, the adjacent ones, and the transmitted beams (for instance H and J on the K dichroics).

For SFJ, it was noticed that the J1 mirror does not allow to put the beam in the theoretical position of the design. If one need to put it in a correct position in order to achieve the correct arrangement of the J pupil, the mirror mount must be translated horizontally along the mirror surface plane. This adjustment requires to drill a new hole for the fixation of this mirror.

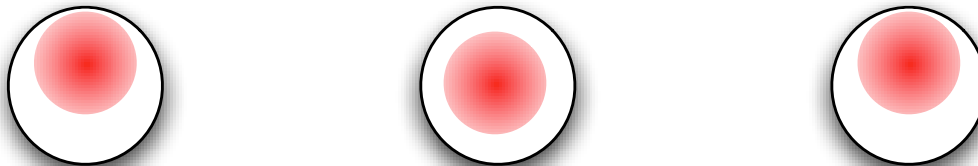
## Beam Vigneting / Input Beams

note : laser beams diameter are oversized by 2mm

### Beam position on input parabolas (J1 / J2 / J3) (front view)



### Beam position on input parabolas (H1 / H2 / H3) (front view)



### Beam position on input parabolas (K1 / K2 / K3) (front view)

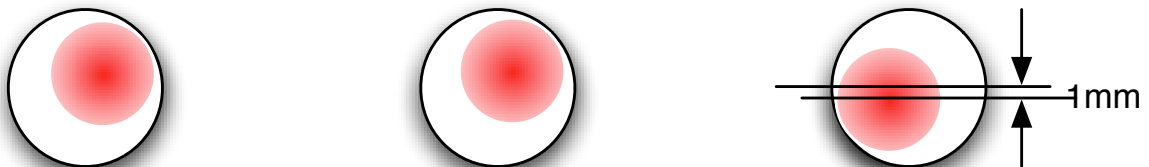


Figure 7: Beam positions at the input parabolae as reported on February 6th 2008.

## Beam Vigneting / Output Beams

February 5th 2008

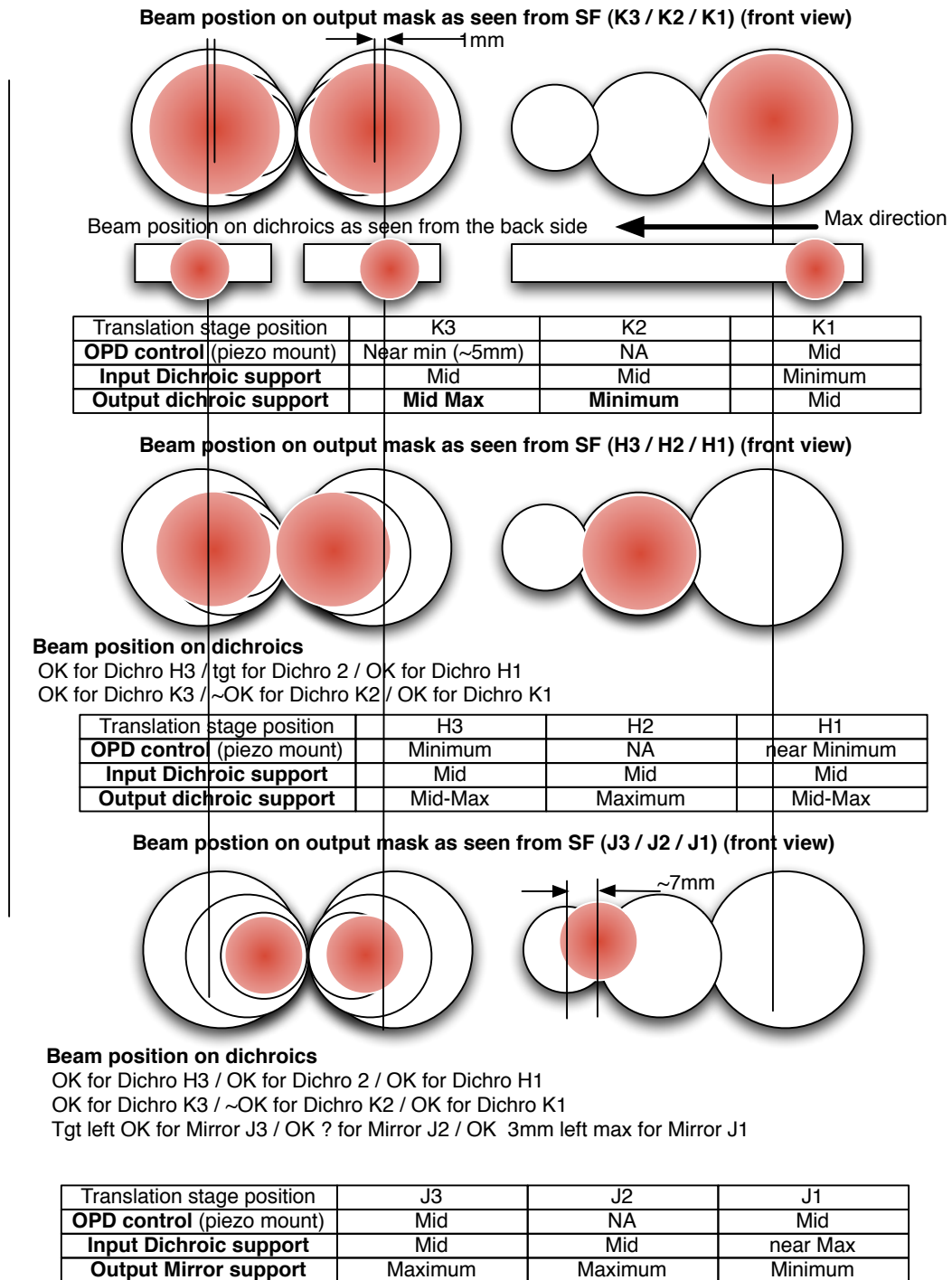


Figure 8: Summary of the beam positions at the output of the spatial filters, as reported on February 6th 2008.

OCA/UNSA LAOG MPIfR/OAA	<b>VLT / AMBER</b>	Doc. No VLT-TRE-AMB-15830-7120
	February 2008 ATF run report <sup>1</sup>	Issue : 1.2
		Date : 16/04/2008
		Page : 18 / 51

## C Characterization of ghosts

### C.1 Mismatch of photometric calibration

The acquisition of the P2VM (pixel-to-visibility matrix) is pivotal in the observing and data reduction scheme of AMBER. Immediately after P2VM calibration, every possible calibration parameters have been obtained. The quality of the raw data observations needed to acquire a P2VM do not obey the prerequisites implied by the concept of a P2VM, described by its mathematical formulas.

In brief, the photometric calibration allows to subtract the continuum from the detected fringes so that the continuum-corrected interferogram is on average equal to zero. The first problem was found when we compared in the continuum obtained actually measured in the interferometric channel from the one which is being subtracted. Fig. 9 shows an interferogram which has been averaged over 1000 frames. Since the fringe phase fluctuations are larger than a fringe period, the fringe modulation disappears and we got a good estimation of the fringe continuum (black line). On another hand, using the P2VM calibration files which allow the ratio between each photometric beam and its counterpart in the interferometric channel to be measured, one see that the computed continuum (red line) does not correspond to the actual continuum.

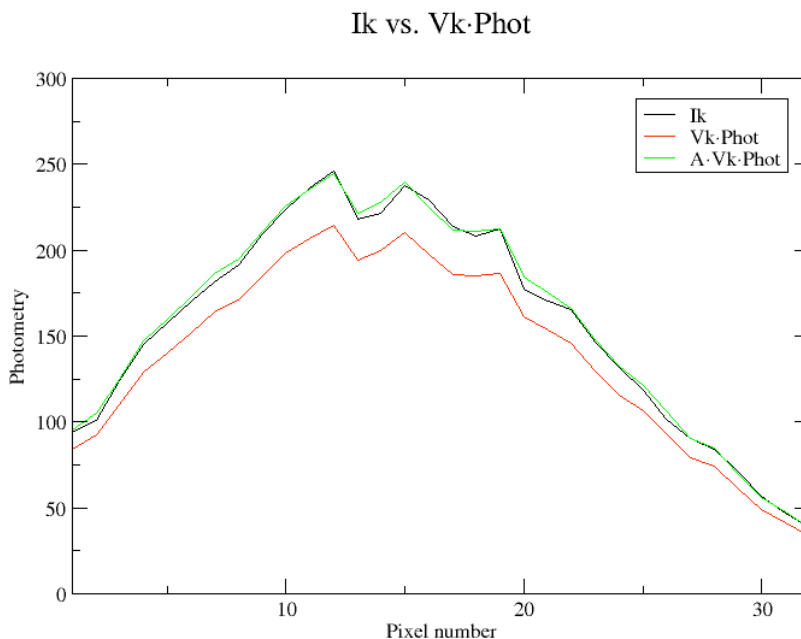


Figure 9: Interferometric channel: continuum measured by averaging 1000 interferograms (black line) compared to the continuum computed by the software for one frame with the photometric calibration (red line). The green line corresponds to the red line multiplied by a constant  $A$ .

The reason for this mismatch is that the assumption that there is no leaks or ghost in other channels is no correct. One way to compensate this is to introduce a multiplicative factor  $A$ , or even better to take into account the cross-talk between the channels in the interferometric/photometric ratios (see Sect. 2 and appendix A).

### C.2 Investigating P2VM calibration files prior to Feb 2008

We have analyzed historic data set to investigate if it possible to detect this cross-talk or ghost in the calibration files produced by the P2VM procedure. Figures 10 and 11 shows two data sets taken respectively in Feb 2005 and Sep 2007 just after the SPG intervention.

OCA/UNSA LAOG MPIfR/OAA	VLT / AMBER	Doc. No VLT-TRE-AMB-15830-7120
	February 2008 ATF run report <sup>1</sup>	Issue : 1.2
		Date : 16/04/2008
		Page : 19 / 51

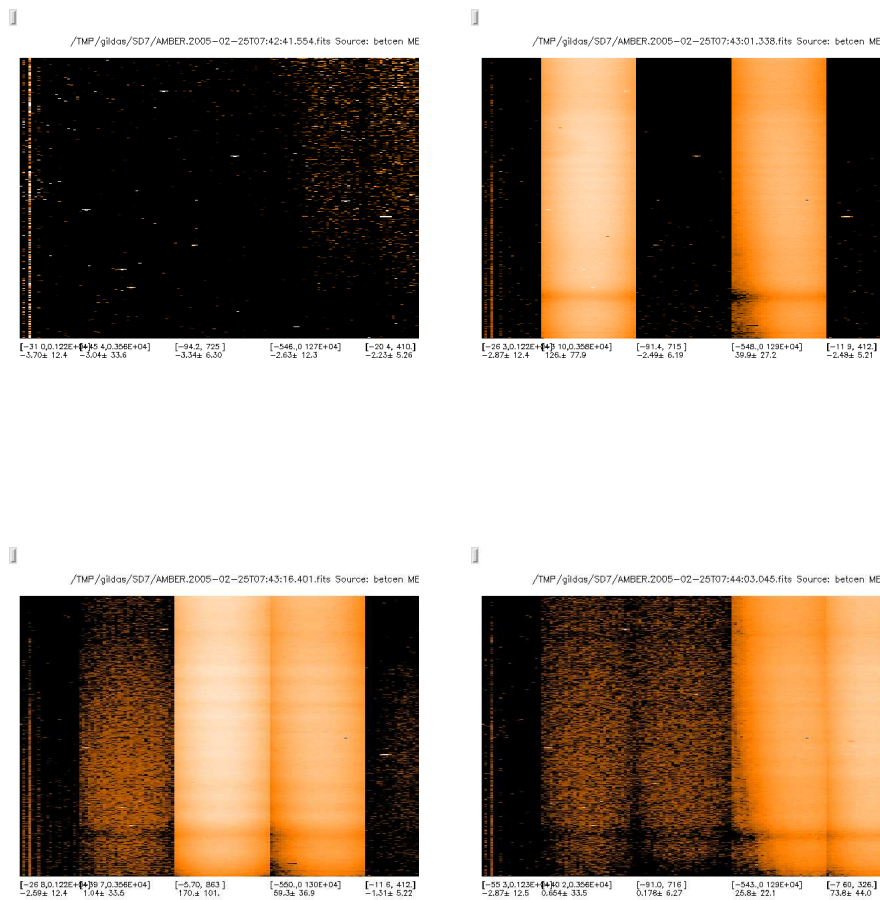


Figure 10: P2VM calibration files obtained in Feb 2005. **Top Left:** DARK. It is not entirely dark on beam 3 : (this does not seem to be remanence of the previous observation—spectral calibration of beam 3). **Top Right:** BEAM #1 . No ghost visible (note that beam 3 is now dark). **Bottom Left:** BEAM #2. Pollution at 0.5% of beam 1 by beam 2 (but this can be remanence) , a hint of something in beam 3 (so this is not remanence). **Bottom Right:** BEAM #3. Pollution at 1% of beams 1 and 2 by beam 3 (if remanence, should have disappeared in beam 1, proving that in left image it was not remanence either)



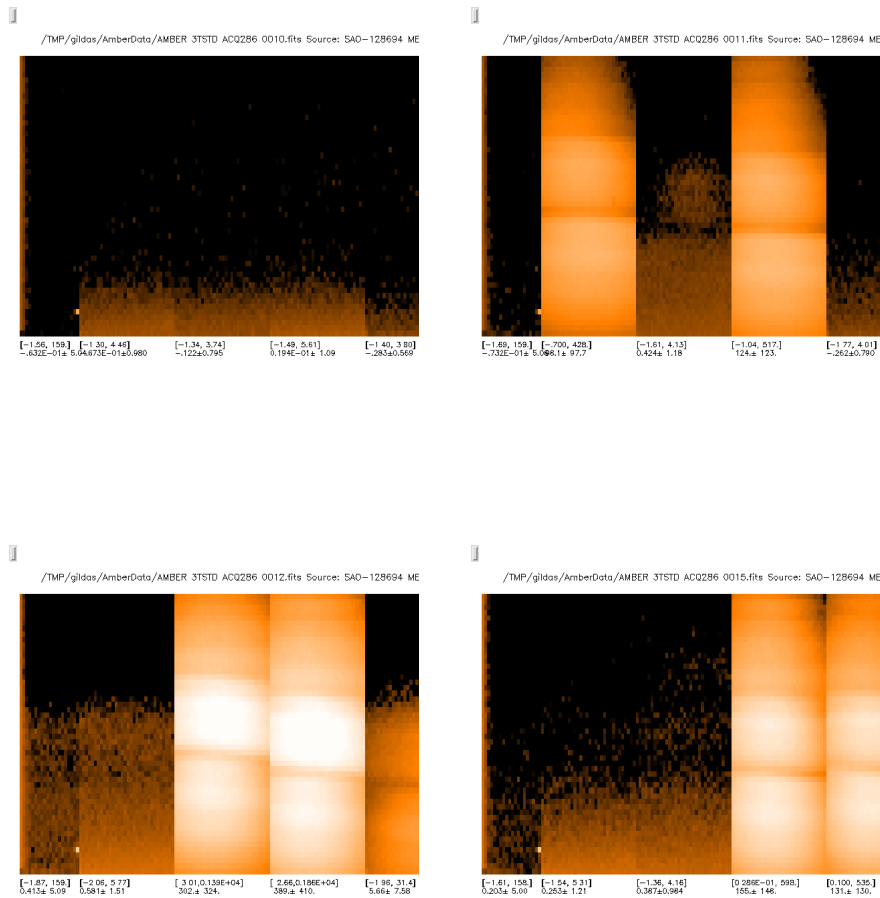


Figure 11: P2VM calibration files obtained in Sep 2007. **Top Left:** DARK. It is dark (except on bottom above 2.3 microns where thermal background emission of the fiber heads and of the lab is present). **Top Right:** BEAM #1. Beam 1 pollutes in H and K beam 2 (0.3%). **Bottom Left:** BEAM #2. Beam 2 pollutes beam 3 very strongly (2%) and, in a much smaller measure (0.2%), beam 1. **Bottom Right:** BEAM #3. Beam 3 does not pollute beam 1 and only very marginally beam 2. (See additional note in text).

OCA/UNSA LAOG MPIfR/OAA	VLT / AMBER	Doc. No VLT-TRE-AMB-15830-7120
	February 2008 ATF run report <sup>1</sup>	Issue : 1.2
		Date : 16/04/2008
		Page : 21 / 51

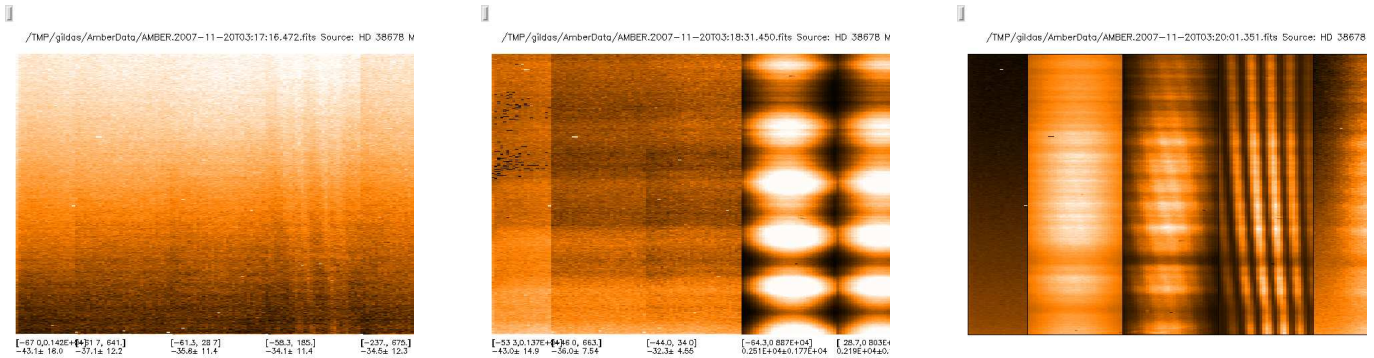


Figure 12: P2VM calibration files obtained in Nov 2007. **Left:** DARK. Some fringes are present in the interferometric channels probably due to remanence effect. **Middle:** spectral file BEAM #3. Frame taken for the spectral displacement calibration. The scale is histogram equalisation to see subtle effects: influence of enlightened beams on the background of dark channels. **Right:** Frame taken for the P2VM Ck value for beams 1-2.

In the following, all images were taken on a mean of all frames in the files. All plots are done with a logarithmic transfer curve to flatten the dynamics. Black is 0.1 ADU, white is 1000 ADU. On all presented images, from left to right we have :

1. masked channel (20 pixels wide, never illuminated)
2. Photometric Channel 1 (32 pixels wide)
3. Photometric Channel 2 (idem)
4. Interferometric Channel (idem)
5. Photometric Channel 3 (idem)

The vertical axis shows the spectral signal from shorter wavelength (bottom) to longer wavelengths (top) for LR mode, the reverse for MR mode. Due to a bug in the gildas interface to the `amdlib` software used here for displays, the wavelength information on the right of the boxes is incorrect for LR mode.

In Feb 2005 data (Fig. 10), one detect a pollution of beams 1 and 2 by beam 3 at the level of 1%. The example given is done with the “Old” Camera, in mode 3T Medium K. Relevant comments are made in the label of each figure. We note that since this dataset was used for the P2VM of the successful Alfa Arae data, the effects depicted here were not seen at the time and thus acceptable.

In Sep 2007 data (Fig. 10), beam 2 pollutes beam 3 clearly at the level of 2%. Theses calibrations were done with the “new” Hawaii camera (no remanence) in mode 3T Low\_JHK. Note also the position of the dark limit between H and K, and its displacement in beams 1 and 3 wrt the position in beam 2 (enormous with today’s tilted slit). This displacement is not the same in all beams, so the crosstalk between beams is also a crosstalk between wavelengths. It will be difficult to get accurate visibilities with such a crosstalk.

A different type of problem is seen in a second set of observations taken in Medium\_K mode (see Fig. 12). In the dark exposure taken before the three files used for computing the spectral displacement (left panel), we note fringes in the interferometric channel. These are due to a remnant feature of the previous observation. It would seem that the camera still has some remanence. Since this kind of frames is used to compensate for pixel biases, any degree of pollution by artifacts will have a severe effect on all the observations. It is advisable to introduce in the AMBER OS a test on each such frames invalidating the data in this case.

OCA/UNSA LAOG MPIfR/OAA	VLT / AMBER	Doc. No VLT-TRE-AMB-15830-7120
	February 2008 ATF run report <sup>1</sup>	Issue : 1.2
		Date : 16/04/2008
		Page : 22 / 51

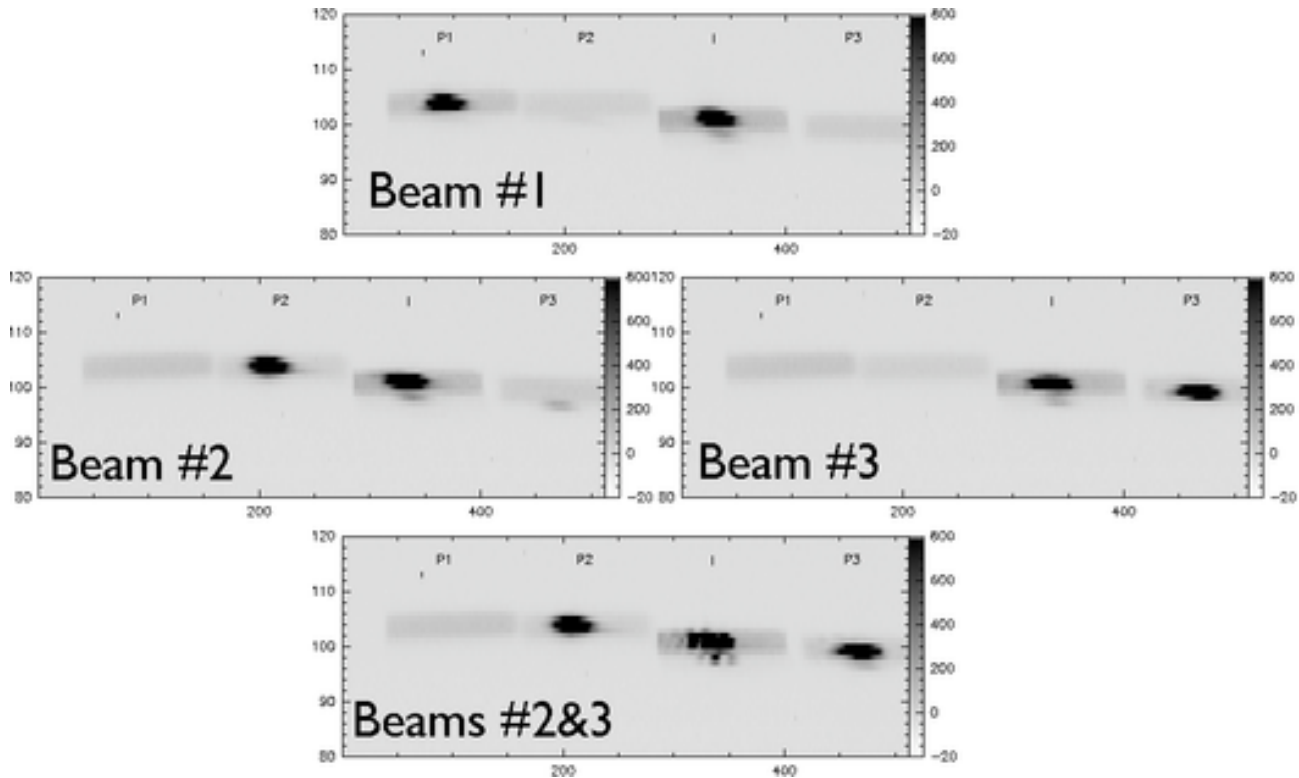


Figure 13: Images of the narrow slit taken at the 0<sup>th</sup> order of the grating showing the shape of non-dispersed beams. From top to bottom, left to right, we have: the image with only beam #1 lightened, same thing with beam #2 and beam #3, then beams #2 and #3 lit simultaneously. Notice the fringe pattern at zero dispersion in the I channel, the fringed ghost two pixels below.

In the middle panel of Fig. 12, which shows the beam #3 enlightened with a spectral modulation for the spectral calibration, the flux variations in the lighted channels (I and P3) change the background in all the other channels, even the masked channel. This is not due to beam pollution but is a known effect of the camera readout, seemingly unavoidable and possibly not entirely taken in account properly in the cosmetics performed in the first steps of the data reduction.

In the right panel of Fig. 12, fringes are visible in the photometric beam 2, and possibly beam 1. Light in beam 3 is due to pollution by beam 2 as in middle panel. The fringe pattern shifts with the piston, proving that this effect is either a global interference pattern in front of the camera, or a ghost of interferometric beam seen in beam 2.

### C.3 Ghosts measured during ATF

All images have been taken with the narrow slit, in the 0<sup>th</sup> order of the grating and a neutral density 10 on the CAU lamp to enable a longer integration time. This long integration time enables the visualisation of the slits itself, even in beams where the shutter is closed, thanks to the background thermal emission of the lab going through the slit.

The images of Fig. 13 show that the slit is very well imaged on the camera, and that the 0<sup>th</sup> dispersion position enable to measure very accurately the beam displacement between the photometric and interferometric beam.

Beam #2 has a clear ghost (6% of flux) in beam #3 (displacement: 2 pixels below). Beam #1 may have a hint of a ghost in #2.

All beams induce a 'second image' in the interferometric beam (2 pixels below). This double image being common to all beams must arise in internal reflections in the beamsplitter. When 2 beams are lit, as in the #2-#3 image we have a second set of (less bright) clear fringes 2 pixels below the first one. This ghost represents 6% of the incoming flux (but its relative importance may change with the wavelength when the flux is dispersed, as it is in normal AMBER operation). The differential path of these reflections in the beamsplitter being small, the fringes are just displaced by

OCA/UNSA LAOG MPIfR/OAA	<b>VLT / AMBER</b>	Doc. No VLT-TRE-AMB-15830-7120
	February 2008 ATF run report <sup>1</sup>	Issue : 1.2
		Date : 16/04/2008
		Page : 23 / 51

$\lambda/4$ .

When we add dispersion, the interferometric channel will thus see superimposed 2 sets of fringes, the normal one plus a second, much fainter, with a different phase, one spectral resolution element (2 pixels) below. Normally this displacement should not change with the spectral dispersion.

We have been able to take into account quite successfully the presence of the ghosts in the data reduction tools we developed specifically for this ATF run (see Section 2), and these algorithms should be ported to the standard data reduction tools for optimal use of AMBER. However this software compensation cannot reach the same level of precision that would be attained by replacing the optical element which creates the ghost in the first place<sup>3</sup>. In particular the ghost fringes seen above cannot be compensated by software and will induce at minimum a contrast loss.

## C.4 Conclusions and recommendations

The most probable explanation of the observed ghosts is the effect of the device inside the spectrograph dewar that arranges the beams on the camera. A set of three small adjacent mirrors redirects the 3 photometric beams on the detectors. The widths of these mirrors is very close to the width of the incoming beams and a small misalignment of one of the pupils on these mirrors lead to a leak to the adjacent mirror. According to the pupil alignment, a different amount of leak may occur, and it seems that the last pupil alignment in October 2006 introduced a larger leak on the beam 3. In any case it is not sure that the beam is not a little bit larger than the element-mirrors leading to a slight ghost on both adjacent mirrors.

This ghost effect should be measured and compensated by the amdlib software for the P2VM calculation. However, the large displacements in data taken between Sep 07 and Jan08 are not retrievable easily, at least not automatically (perhaps can be entered by hand), and will reduce the number of useable data channels. Removal of these ghosts and removal of the spectral displacement is badly needed. Besides, we need to have a value returned by the amdlibComputeP2VM routine used in the amber observation software to tag invalid P2VM observations which exhibits ghosts effects above a sensible value (0.5% for example).

The new alignment performed after the Jan 2008 SPG intervention allowed to decrease the cross-talk between photometric beams, but a ghost remains in the interferometric channel which comes from the interferometric channel itself (probably a reflection on the common beamsplitter used to extract photometric beams).

The camera change is believed to have solved the remanence problem, although we seem to see the contrary in fig. 12 (upper panel). At the moment, no remanence is taken into account in the data reduction program, for lack of removal method (before or after which cosmetics, with what value, etc...).

---

<sup>3</sup>which remains to be identified.

## D Optical stability

### D.1 Output beams

#### D.1.1 Medium term stability survey during the ATF operation

A survey of the beam positions and of the beam fluxes was performed during the last week of the ATF operation. No significant drifts were observed within a time scale of a few days. In any case during the second part of the ATF operation, when the main alignments were completed, we did not need any more intervention in the laboratory to re-adjust the beams. Mainly it must be noticed that for the output beams the requirement used by the Paranal team for the adjustment is overestimated. Using the related software alignment tool, the green dot means that the beam is properly aligned, the orange one means acceptable, a re-alignment can be required latter, and only the red dot imposes an immediate re-alignment. It is highly preferable to perform the verification from a control room and to avoid any disturbances on the bench.

Left and middle panels of Fig. 14 show respectively the variation of the beam positions in K, H and J in the X and Y direction, and the right panels display the variation of output fluxes for the different bands. This survey was performed from February 6th to February 13th. On February 12th, the polarizers were removed explaining the significant improvement of the flux level.

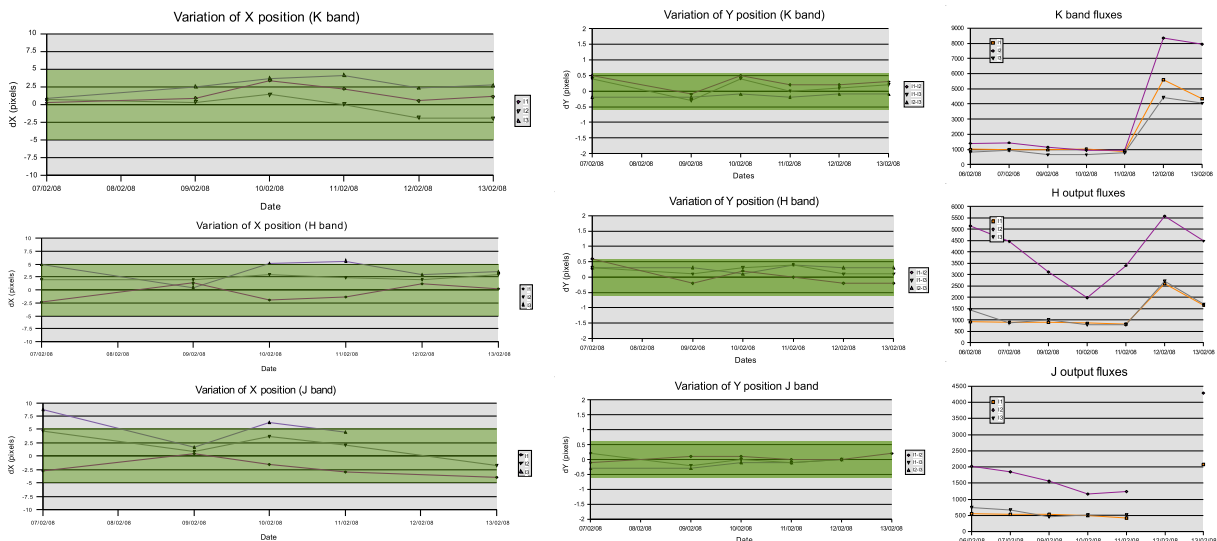


Figure 14: Optical stability of AMBER. Left panels: X-positions of the output beams during the ATF week. Middle panels: Y-positions of the same beams. The green zones correspond to a tolerance of 10% contrast loss (see Fig. 15). Right panels: fluxes during the ATF week. The flux increase at the end of the week corresponds the removal of the polarizers (gain of factor 2 to 3) and the change of the internal source (gain of about a factor 2).

On Fig. 15, we plotted on the left the beam shapes for a typical value of FWHM of 23 pixels in X-direction (solid line) and of 1.6 pixels in Y-direction (dashed line). On the right part of the figure is represented the contrast loss due to overlapping mismatch in pixels. One see that less than 10% losses requires overlapping at the level of 5 pixels in X and of 0.6 pixels in Y. The fact that the positions are within the green zones in Fig. 14 shows that during the ATF run the beams were always within specifications.

Our understanding is that the effort done by Paranal to achieve a better stability of AMBER by cutting and strengthening the optomechanical elements were fruitful.

#### D.1.2 Sensitivity to vibrations

When we were looking for the origin of the fluctuations of the visibility (see Sect. 3.3.1), we have recorded a set of 1000 frames with the grating in the 0<sup>th</sup> order in order to monitor at relatively high frequencies (more than 10Hz) the

OCA/UNSA LAOG MPIfR/OAA	<b>VLT / AMBER</b>	Doc. No VLT-TRE-AMB-15830-7120
	February 2008 ATF run report <sup>1</sup>	Issue : 1.2
		Date : 16/04/2008
		Page : 25 / 51

motion of the output beams.

The result of this test is reported in Fig. 16. The variations are at maximum within a fraction of pixels, unable to explain visibility variations of a few percent. We concluded that the output beams are not responsible of the visibility variations seen.

## D.2 P2VM stability

The stability of calibrations beams have characterized during the last ATF night (see Fig. 17). Left subfigures correspond to the P2VM acquired at the begining of the night, whereas the right ones to the end of the same night. The images at the top of the figures shows the carrying waves. Fringes of baselines 1-2 and 1-3 have not moved significantly whereas the fringe of baseline 2-3 show different pistons. However the analysis of the P2VM using P2VM modeling reported in graphs below show that the envelope and frequencies have not changed. Only the phase has changed.

This is due probably to translation stages of the input dichroics which have been found very unstable. This is a well known problem reported in some PPRS. When used too many times, then the OPD is unstable. However we think it would be possible to make the P2VM calibration process unsensitive to the piston so that this problem should not be a problem. This needs further investigation.

## D.3 CAU stability

We did a series of experiment on the CAU to test its stability. During the search for the origin of visibility fluctuations, we noticed that the visibility measurements were very sensitive to some elements of the CAU, especially the large CAU parabolic mirror.

In Fig. 18, we have recorded an exposure (1000 frames) on the CAU source while touching different mechanical supports of the CAU. We found that the mount of the large CAU parabolic mirror (identified on Fig. 19) was very sensitive to mechanical impacts. We think that it may be the source of the instabilities seen when we were looking to the effect of polarizers (see appendix G).

## D.4 Conclusion: on alignment requirements and health checking

We recommend to relax the alignment requirements to 8 pixels (see fig. 15), in order to avoid too frequent interventions in the laboratory. However, this requirement holds for each pair of beams, at each wavelength. We recommend that in the p2vm computation a fit of the position of each beam, as seen in the interferometry channel, as a function of lambda, be performed, that these values be used as health check, and that a warning be issued each time a significant percentage (5%) of wavelengths are above these specs.

We also recommend to check the fixation of the large CAU parabolic mirror.

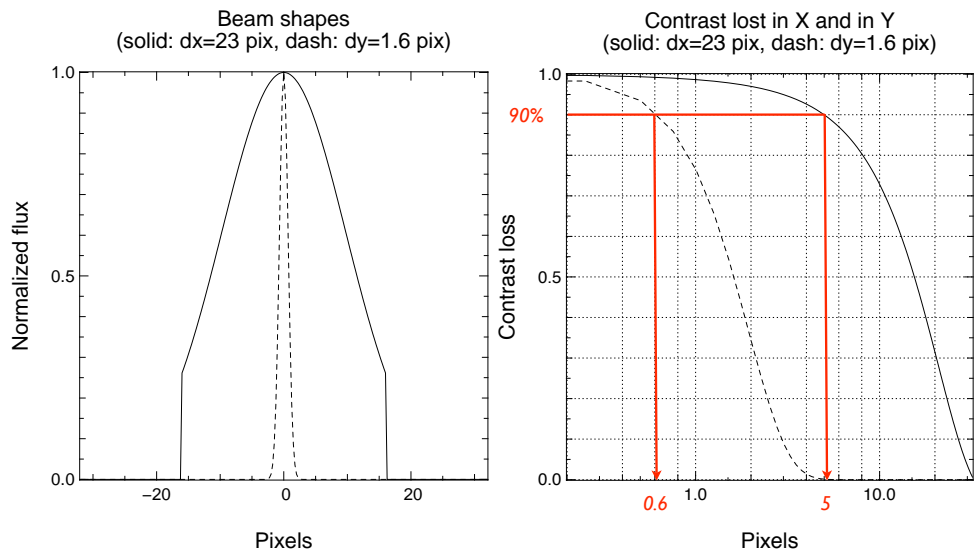


Figure 15: Tolerance of the overlapping output beams. Left: beam shapes for the X direction (solid) and Y direction (dashed). Right: tolerance for the contrast loss in the X direction (solid) and the Y direction (dashed).

OCA/UNSA LAOG MPIfR/OAA	VLT / AMBER	Doc. No VLT-TRE-AMB-15830-7120
	February 2008 ATF run report <sup>1</sup>	Issue : 1.2
		Date : 16/04/2008
		Page : 27 / 51

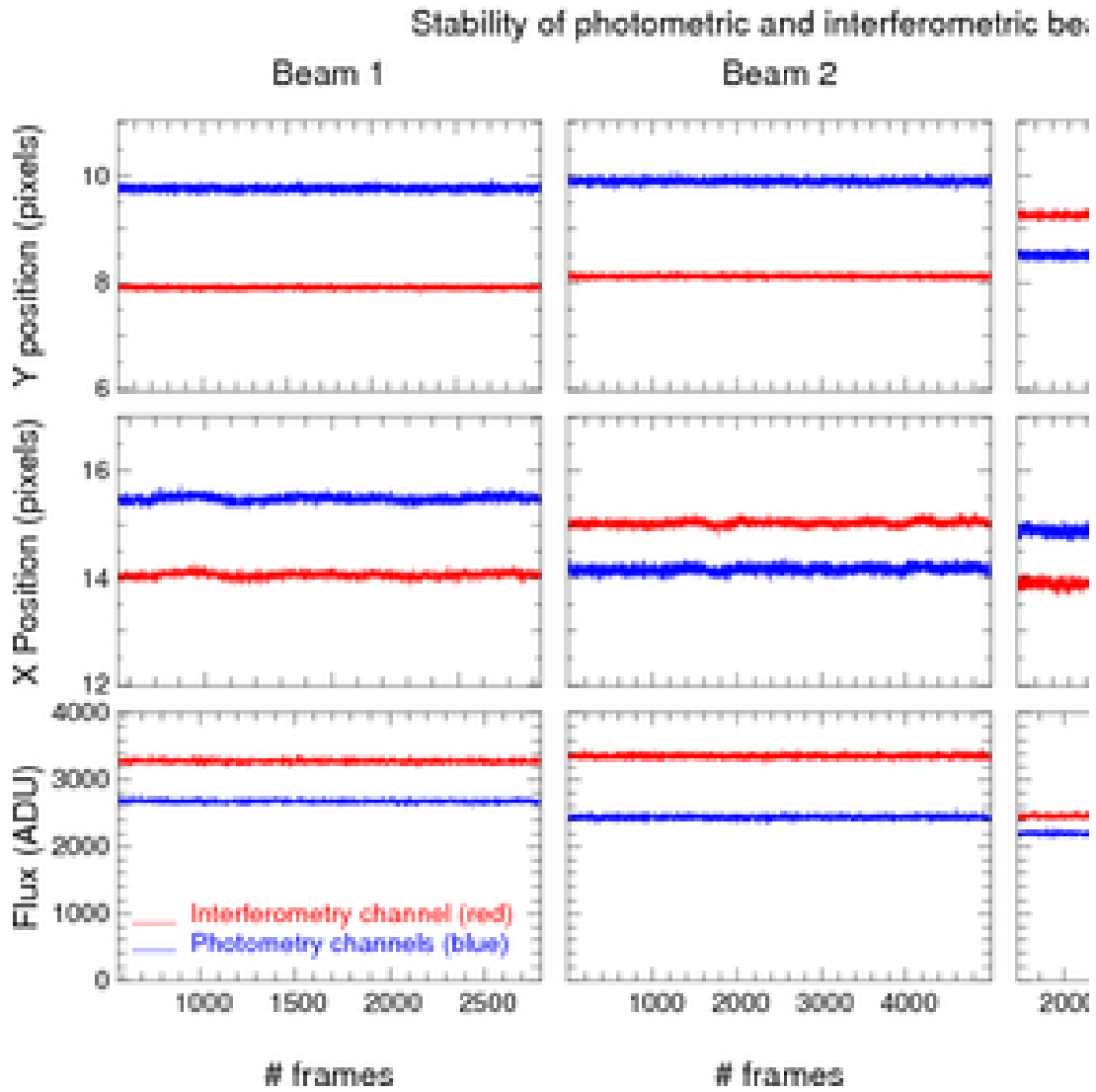


Figure 16: Stability of output beams in X- and Y-position and flux with DIT of 20ms. Top and center panels are Y- and X-positions of the 3 beams in their photometric channels. Bottom panels are the flux levels. The variations are at maximum within a fraction of pixels.



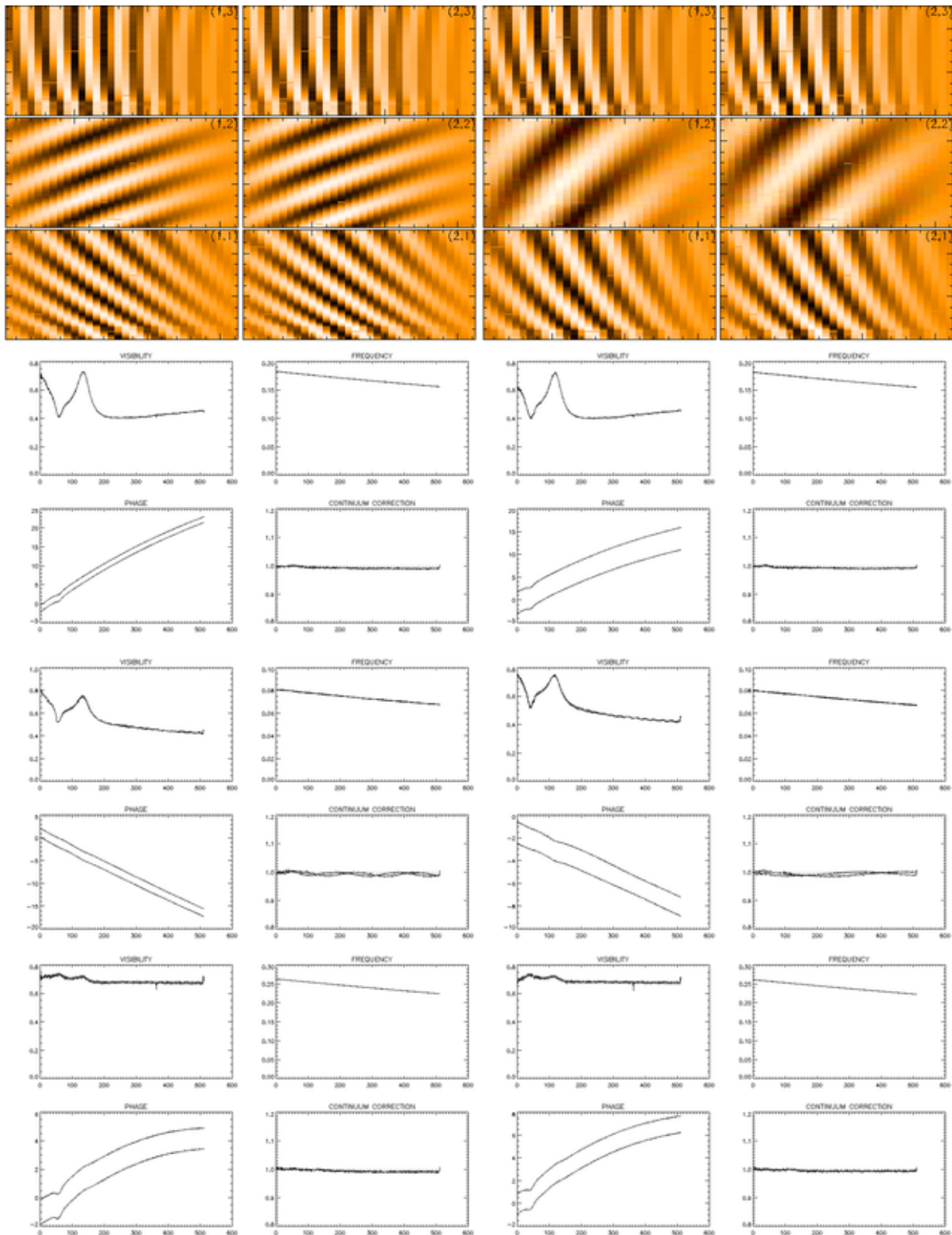


Figure 17: P2VM stability illustrated by the P2VM taken at the beginning of the sky tests (left) and at the end (right) without changing the spectral configuration. See text for details.

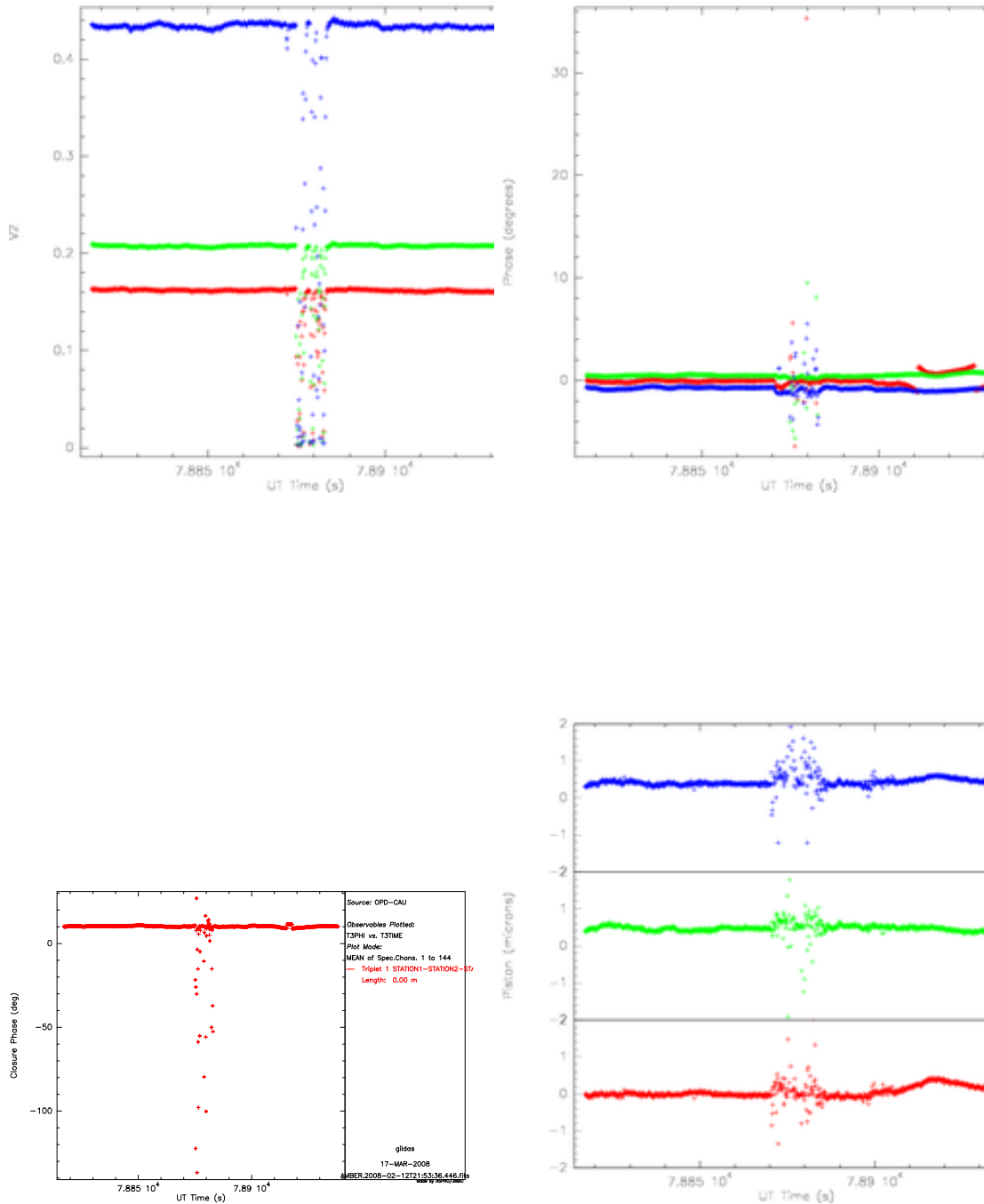


Figure 18: Test of the CAU stability. During observation of the internal source, several optical mounts of the CAU were touched in order to detect any special sensitivity to external stimuli. Upper left: squared visibility; upper right: differential phase; bottom left: closure phase; bottom right: piston. One sees the impact of touching the CAU large parabolic mirror and its relaxation time.

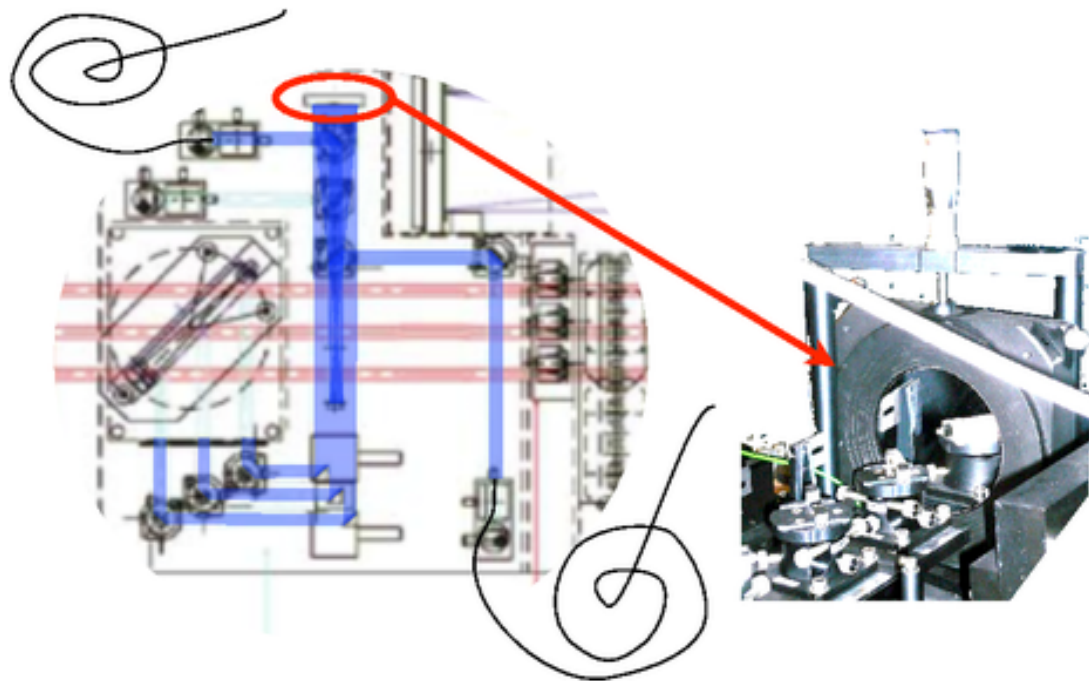


Figure 19: Layout of the CAU (calibration alignment unit) with a picture of the CAU large parabolic mirror that we suspect to be unstable and to generate OPD instabilities.

OCA/UNSA LAOG MPIfR/OAA	VLT / AMBER	Doc. No VLT-TRE-AMB-15830-7120
	February 2008 ATF run report <sup>1</sup>	Issue : 1.2
		Date : 16/04/2008
		Page : 31 / 51

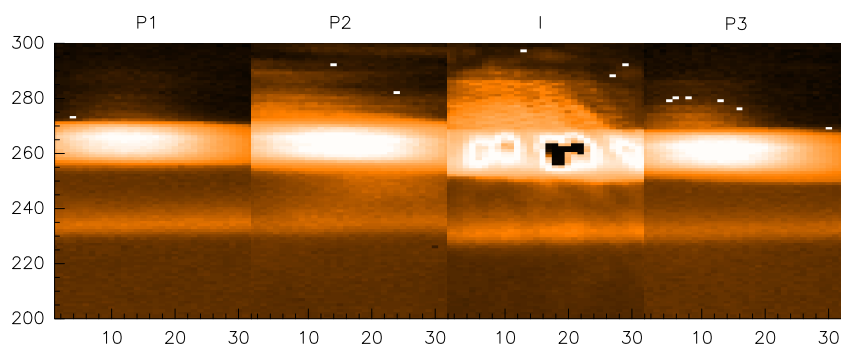


Figure 20: Image of the slit in September 2007. the image is very defocussed (4 pixels HPBW instead of less than 2 normally), and a ghost images are seen above and below the slit image up to 30 pixels away.

## E Analysis of the spectral resolution

### E.1 Spectral shifts between photometric and interferometric channels

The spectrograph is well-aligned. The spectral shift between photometric channels and the interferometric ones is characterized and should not be recomputed each time (gain of observing time).

The spectral shift is primarily due the combination of the position of the slit (large, narrow, etc) and of a small angle between the optical components that fold the 3 photometric beams on the camera (3 glued total-reflexion prisms). The figure 13 show such images of the slit. At the worst, this combination changes by a small amount every time the spectrograph is opened. To our knowledge, this defines only 3 periods: 2004–Sep, 2007; Sep, 2007–Jan, 2008 and Feb, 2008–present.

The repositioning of the slit by the slit wheel motor *seems* (TBC) to be sufficiently accurate to insure that the slit+folding device setup did not change during these periods.

The displacement of *the image of the slit* on the camera measures the main displacement. This can be done only once each time the spectrograph is opened, and could be done in the following manner:

1. take 3 exposures full frame images of the narrow slit, one beam lit at a time, grating at 0 order.
2. sum each image on the X axis (taking care of bad pixels. Flat is not needed)
3. on these 3 vectors, fit two gaussians of FWHM $\sim 32$ pixels. Their position will serve as a marker of the position of each beam;
4. average a few long (1 min) exposures full frame images of the narrow slit, **all shutters closed**;

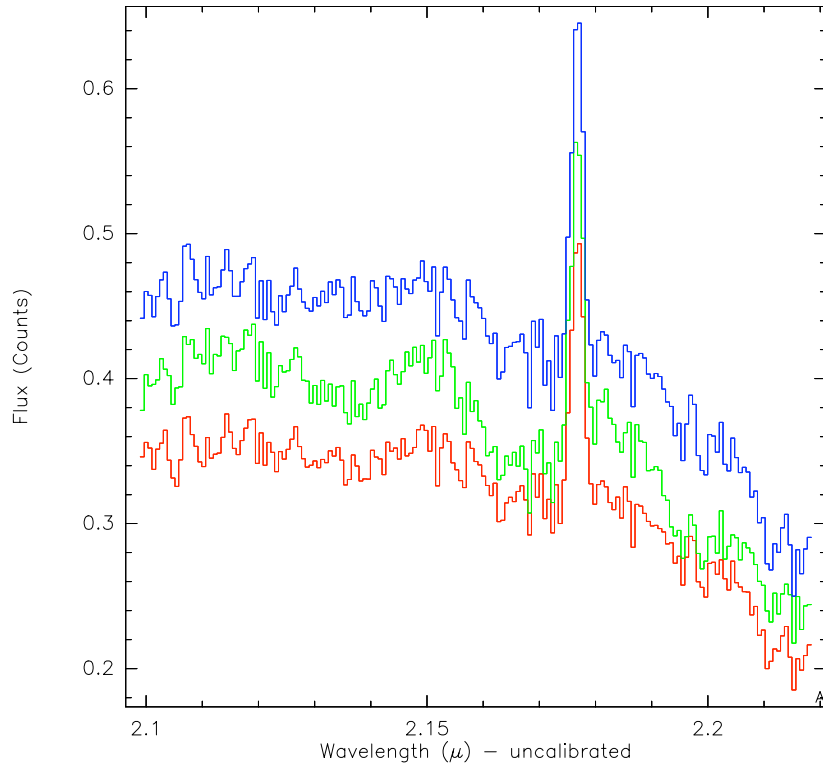


Figure 21: Spectra of  $\alpha$  Arae measured in Feb 2005 during Science Demonstration Time. The curves corresponds to beam of each telescopes and have been shifted with a fixed values computed at a different date.

5. extract 4 strips in the Y (lambda) direction, of 64 pixels wide, centered on the positions of the beams found before (taking care of bad pixels. Flat is not needed);
6. sum each strip on the Y axis, fit a gaussian (of a few pixels wide) in each. The displacement of the gaussian positions of strips 1,2 and 4 wrt. strip 3 is the displacement sought. The width of the gaussian is an indication of the quality of imaging of the slit onto the camera (hence the spectral resolution).
7. to evaluate the *quality of the focussing of each beam* the same procedure can be reproduced with one beam lit at a time.

We have done measurements during our ATF stay, and have found old images of the slit taken in 2004, permitting also this kind of measurement. Table 1 summarizes these values.

Table 1: Displacement of the photometric channels with respect to the Interferometric channel (in pixels).

Period	P1	P2	P3	Notes
2004-Aug2007	+0.873	+2.064	+0.472	1
Sep2007-Jan2008	+2.000	+2.576	+0.263	2
Feb2008-Present	+3.008	+2.850	-1.319	3

Notes of the table:

1. These 2004 values seem to hold at least until 2005 Feb. It is necessary and easy to check that it holds until Sep07.
2. Based on Nov07 measurements (SPECPOS frames). Slit was **very** tilted and slit badly focussed (See fig 20 and appendix C comments).
3. Values should be measured again on background-illuminated image of the slit. We believe these are however good values for data reduction purposes.

OCA/UNSA LAOG MPIfR/OAA	VLT / AMBER	Doc. No VLT-TRE-AMB-15830-7120
	February 2008 ATF run report <sup>1</sup>	Issue : 1.2
		Date : 16/04/2008
		Page : 33 / 51

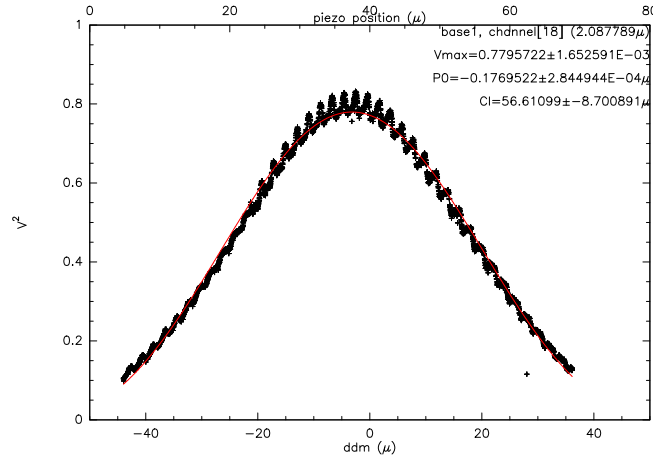


Figure 22: Typical extinction figure obtained in the K band region during our piezo scan. The red line is the fit of the extinction function whose parameters are available in the upper right corner of the box.

The 2004 values seem to hold at least until 2005 Feb, 25 since they work well with  $\alpha$  Arae measurements (see Fig. 21). It is necessary and easy to check that it holds until Sep 2007.

During the replacement of the infrared Hawaii detector in Sep, 2007, a slight defocus and tilt of the slit image was introduced, which was not corrected until Feb, 2008. During this period, the image of the slit on the camera worsened severely, as seen in fig 20. Such defocussing of the slit induces a loss of spectral resolution, and the extinction of the visibility with the piston (sect. E.3 worsens: in LR mode, the maximum tolerable piston drops to  $\pm 20$  microns).

Please note, that **subpixel** shifting, as it is done in amdlib (and the author does not see how it could be done otherwise) introduces biases in spectrum and P2VM in presence of **bad pixels**. We recommend to use integer pixel shift for the moment. (+1, +2, +0 for the old data, +2, +2, +0 for the sep07-Jan08 data ).

In operation, three anamorphed beams pass through the slit. These beams are, if amber is correctly aligned, highly elongated ellipsoidal flux distributions tilted with a very small angle ( $\leq 0.5^\circ$ ) wrt the slit, whose shape can be measured at 0th order with a good precision. Thus, one could in principle apply psf deconvolution on the P1, P2 and P3 spectra, possibly to gain in spectral resolution in the *spectrum*. It remains to be proved that the same could be done in the I channel, taken into account in the P2VM fitting process, and provide a sensible improvement in the results.

## E.2 Spectral calibration in low resolution JHK mode

We performed a Fourier Transform Spectrograph analysis of AMBER's Low JHK spectra by moving incrementally by steps of 0.01 microns the piezos on beams 1 and 3 for each band. Each pixel of the Interferometric region on the camera of amber (32 by 60 pixels in this LR mode) is thus modulated with a period equal to the wavelength it sees. Furthermore the visibility of the 1-2 and 2-3 fringes will vary as a function of piston and will change as the fourier transform of each spectral channel shape.

We acquired four observations of  $10^4$  images, covering piezo displacements of 80  $\mu\text{m}$  with 0.01  $\mu\text{m}$  resolution, with the polarizer present, so the data is perturbed by the phase beating effect depicted in Sect 4.2, and the dispersion law was thus obtained for the H and K regions of the spectrum only. A typical result is depicted in fig. 22, where the phase beating perturbation is clearly visible.

The Dispersion law is found compatible with a linear dispersion of coefficients:

$$\lambda = 2.6917 - 3.2082 \cdot 10^{-2} \times i$$

with  $i$  as the pixel number.

OCA/UNSA LAOG MPIfR/OAA	<b>VLT / AMBER</b>	Doc. No VLT-TRE-AMB-15830-7120
	February 2008 ATF run report <sup>1</sup>	Issue : 1.2
		Date : 16/04/2008
		Page : 34 / 51

### E.3 Calibration of visibility losses due to temporal coherence

Table 2 presents the 'equivalent coherence length'  $\Delta\lambda$  of the extenuation of  $V^2$  as a function of piston 'opd'. It has been computed through the K band by fitting the extenuation law in sinc expected from a square spectral channel of bandwidth  $\Delta\lambda$  and

$$V^2 = V_{\max}^2 \times \left\{ \frac{\sin(\pi \frac{opd}{\Delta\lambda} + P_0)}{\pi \frac{opd}{\Delta\lambda} + P_0} \right\}^2$$

Table 3 is a subproduct of the data reduction used in the measurement. It shows the maximum piston measurable with the Low\_JHK spectral resolution in case of good S/N.

OCA/UNSA LAOG MPIfR/OAA	<b>VLT / AMBER</b>	Doc. No VLT-TRE-AMB-15830-7120
	February 2008 ATF run report <sup>1</sup>	Issue : 1.2
		Date : 16/04/2008
		Page : 35 / 51

Table 2: “Coherence Length” and central wavelength of each spectral channel in the K band

LR Spectral Channel number	$\lambda$ (microns)	$\Delta\lambda$ (microns)
1	2.6596	46
2	2.6275	51
3	2.5954	53
4	2.5633	52
5	2.5312	51
6	2.4992	52
7	2.4671	55
8	2.4350	58
9	2.4029	59
10	2.3708	58
11	2.3387	57
12	2.3066	55
13	2.2745	57
14	2.2425	59
15	2.2104	59
16	2.1783	56
17	2.1462	58
18	2.1141	57
19	2.0820	59
20	2.0499	50
21	2.0179	54
22	1.9858	58
23	1.9537	33

Band Channel number	Maximum Measurable Piston (microns)
J	$\pm 20$
H	$\pm 27$
K	$\pm 43$

Table 3: Maximum measurable OPD between beams in Low resolution mode.



OCA/UNSA LAOG MPIfR/OAA	VLT / AMBER	Doc. No VLT-TRE-AMB-15830-7120
	February 2008 ATF run report <sup>1</sup>	Issue : 1.2
		Date : 16/04/2008
		Page : 36 / 51

## F Internal light sources and effect on closure phases

### F.1 Analysis of internal sources

We investigated how the CAU sources, also called RAS, could be simplified and understood. We explain below some tests which were performed.

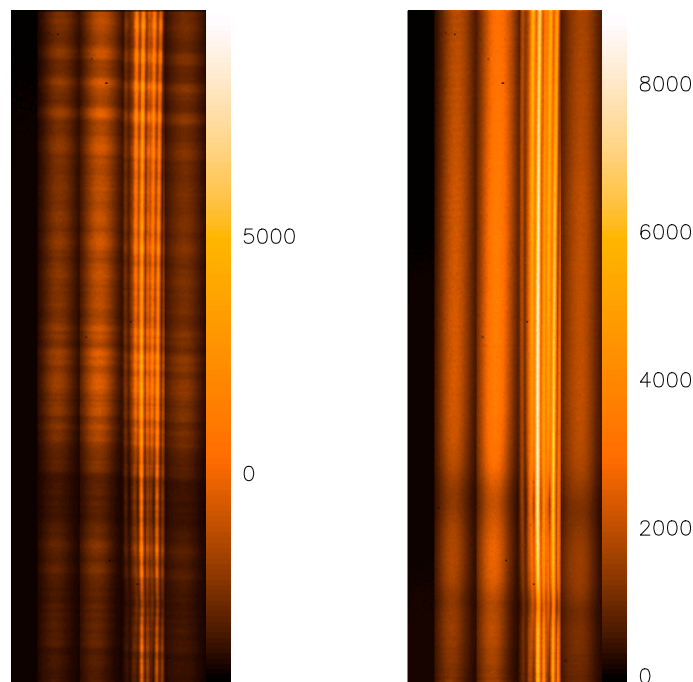


Figure 23: AMBER MR data obtained with the current source (left) and with the new proposed setup (right). See text for details.

- RAS dichroics effects:** For tests the RAS has been replaced by a laboratory source directly connected to the K band fiber of the CAU. In this condition, while the K band dichroic of the RAS is shunted, the modulation of the flux in all photometric channels is significantly reduced and is not detectable any more in the raw data in MR (see Fig. 23). LR image in JHK in this condition allows a detection for all bands. The signal in J and H bands is then highly affected by the fact that the CAU dichroic acts in this test setup, in reflection while it is supposed to be operated in transmission for this spectral range. One can retrieve the reflection curve of the dichroic presented in VLT-TRE-AMB-15830-1010 section 9 (AMBER OPM test report).
- CAU fibers:** It has been observed for a long time by AMBER operators than the 2 CAU fibers suffer from incorrect superposition, as the H fiber seems to be moving and requires some readjustments. This misalignment lead to non-zero phase closure measurement on the CAU, with an unstable value. The measurements done with a laboratory source, shows that a single K band fiber is able to provide the illumination for all wavelengths. Even if the core of the K band fiber can be resolved by the AMBER setup, this effect is properly taken into account by the calibration procedure of the P2VM. If the CAU remaining dichroic is replaced by a mirror, then the flux in all bands are sufficiently balanced with a suitable transmission. We recommend to replace the CAU dichroic and its support by the equivalent mirror and support which deflects the light coming from the H band fiber. Then we keep only one fiber (K band Verre Fluore fiber) for the CAU and to bypass the 2 dichroics of the calibrations sources (RAS and CAU).

### F.2 Effect on closure phase calibration

Measurements showed that the closure phase signal was corrupted. We realize that by shutting down the remote alignment source (RAS) JH fiber, the K spectrum becomes very different. Residual K band light the RAS JH fiber

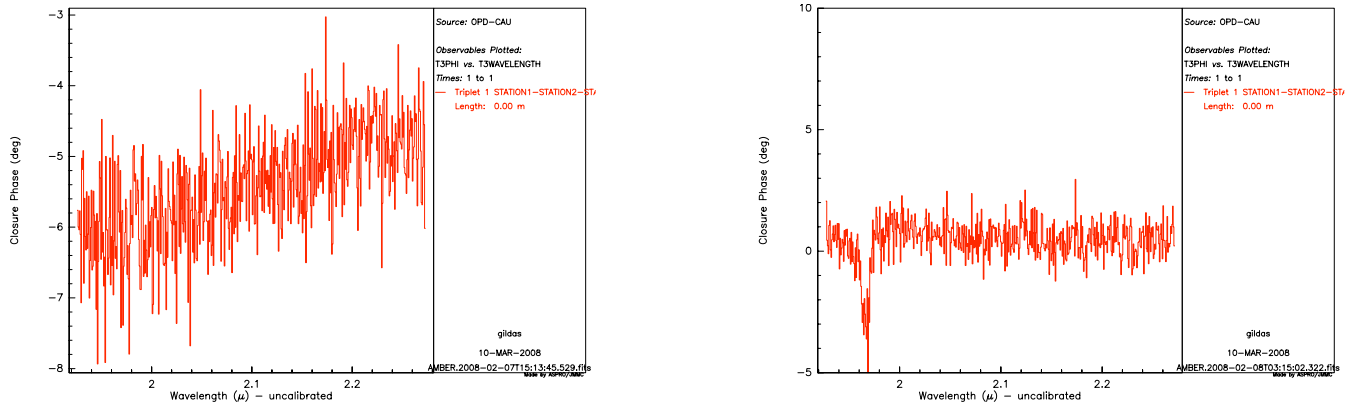


Figure 24: Closure phases measured on the internal source in the K band, left leaving the RAS open with residual K light, right with the RAS closed.

polluted the K source. Therefore the instrument was seeing a binary made by the strong K fiber and the residual K light going through the JH fiber. By shutting down the RAS light leads to a closure of  $0^\circ$  all over the K band (see Fig. 24).

OCA/UNSA LAOG MPIfR/OAA	VLT / AMBER	Doc. No VLT-TRE-AMB-15830-7120
	February 2008 ATF run report <sup>1</sup>	Issue : 1.2
		Date : 16/04/2008
		Page : 38 / 51

## G AMBER polarizers

The polarizers were found to be at the origin of the phase beating and partly at the origin of visibility fluctuations of the AMBER instrument. In this appendix, we describe the polarizers and present some measurements made when looking for visibility fluctuations.

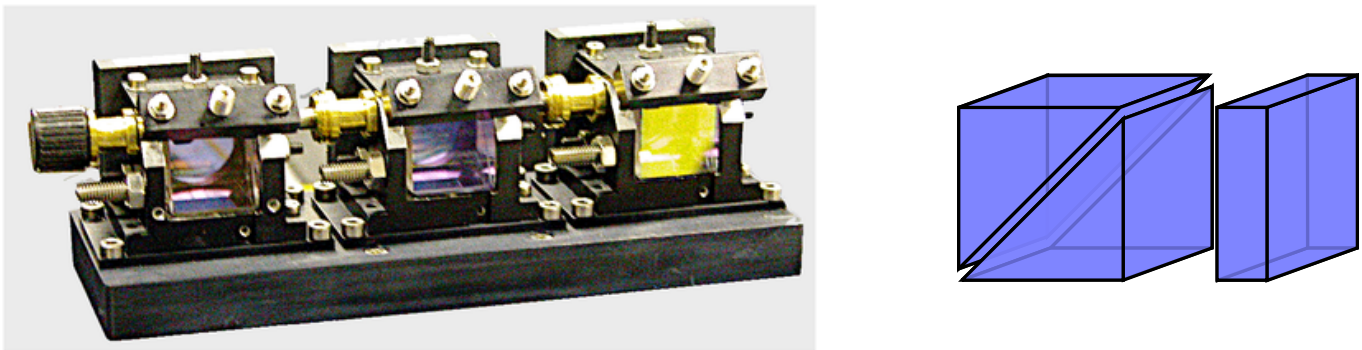


Figure 25: AMBER polarizers (one for each beam) in their mechanical support (left). Each polarizer is made of 2 prisms and a glass blade. The air blade between the two prisms is kept parallel by the mechanical support.

### G.1 Polarizers current design

In the *OPM Warm Optics Design Report* (doc. VLT-TRE-AMB-15830-1001, see [RD 5]<sup>4</sup>)

#### 3.6 POLarization module

Product tree list : AMB-OPM-POL-(PL1,PL2,PL3)-(POL,CBL)

.../...

The maximum defect with respect to the mean thickness of the 3 blades POL-(PL1,PL2,PL3)- CBL must be lower than +/-100 microns.

The beam deviation of the delivered polarizer ( $> 1'$ ) is not compatible with the +/-5" specification imposed by the differential observations (see OPM LLS [3]). This deviation is then minimized by the adjustment of the two prisms constituting the polarizer, the two latter being dissociated. This allows to control the prismatic air layer at the interface. In addition, to be compatible with the differential chromatic OPD specifications, a prismatic blade needs to be added for each polarizer. The complete definition of the blades is given in the OPM Test Report.

In order to ensure a good parallelism between the two opposite internal faces after the dissociation of the prisms which constitute each polarizer, a plastic wedge of 0.12 mm is introduced between these two prisms. The angle formed by this separation needs to be stable within 3.5" during the observations.

In the *OPM Warm Optics Test Report* (doc. VLT-TRE-AMB-15830-1010, see [RD 6]<sup>5</sup>).

#### 13 Manufacturer delivery of the polarizers POL

<sup>4</sup>Available at [http://amber.obs.ujf-grenoble.fr/PLAIN/pae/Documents\\_PAE/Documents/7\\_TRE\\_OPMODR.pdf](http://amber.obs.ujf-grenoble.fr/PLAIN/pae/Documents_PAE/Documents/7_TRE_OPMODR.pdf)

<sup>5</sup>[http://amber.obs.ujf-grenoble.fr/PLAIN/pae/Documents\\_PAE/Documents/9\\_TRE\\_OPMTR.pdf](http://amber.obs.ujf-grenoble.fr/PLAIN/pae/Documents_PAE/Documents/9_TRE_OPMTR.pdf)

OCA/UNSA LAOG MPIfR/OAA	VLT / AMBER	Doc. No VLT-TRE-AMB-15830-7120
	February 2008 ATF run report <sup>1</sup>	Issue : 1.2
		Date : 16/04/2008
		Page : 39 / 51

.../...

### 13.2.2 After reception of the polarizers

Measurements and simulations were performed by Yves Bresson, OCA. They show that the air blade located between the two prisms constituents of each polarizer must be parallel in order for the assembly polarizer and associate compensating blade to respect the chromatic dynamic OPD specifications. A peeling off of the two prisms constituents of the polarizer from the initial mounting delivered by the manufacturer was required in order to insert a plastic shim (with an opening for the optical beam) between them.

.../...

### 14.3 AMB-OPM-POL optical pre-adjustment

.../...

#### 14.3.2 Principle of the assembly and of the compensation

The polarizer is composed of two prisms in calcite. In order to ensure a good parallelism between the two opposite internal faces after the dissociation of the prisms which constitute each polarizer, a plastic shim of 0.12 mm is introduced between these two prisms. A first prism leans inside the mount on six iso-static points constituted by 3 tips on the lower plate, 2 others for the orientation and a reference position [4].

The internal face of the second prism leans on the plastic shim via 3 points constituted by a tip on the lower plate and 2 lateral tips whose one allows the rotation of the prisms along the optical axis (range : +/- 0.5 mm). This prism is clamped by a corner plate guided between two sticks with a spring toe.

Considering the characteristics of the prisms in terms of parallelism and thickness differences, we have inserted compensating blades in order to correct these defaults and to be compatible with the OPD specifications. These compensating blades are mounted in cylinders which can be rotated along the optical axis.

Zemax simulations give the associated chromatic dynamic OPD as a function of the optics characteristics and positions and of the measured beam deviations.

## G.2 Influence of polarizers on the AMBER observables

Figures 26 and 27 shows the square visibilities measured respectively with and without the AMBER polarizers. It is interesting to note that the fluctuations of the visibilities seem to come from varying periodic oscillations with wavelength appearing and disappearing in the visibilities. These oscillations disappeared totally when the polarizers are taken out of the instrument. However the averaged visibility decreases to a level of 0.2 or two baselines and 0.4 for the third one.

Our understanding of this phenomenon is that the air blade between the two prisms of each polarizer is acting as a Fabry-Perot interferometer. Applying Eq. (1) to the number of oscillations seen in a Fig. 26 gives the following Fabry-Pérot thickness:

- Baseline 1-2:  $\approx 2.8$  periods in  $\Delta\lambda = 0.1 \mu\text{m}$  gives a thickness of  $58 \mu\text{m}$ .
- Baseline 1-3:  $\approx 2.2$  periods in  $\Delta\lambda = 0.1 \mu\text{m}$  gives a thickness of  $45 \mu\text{m}$ .
- Baseline 1-2:  $\approx 4.9$  periods in  $\Delta\lambda = 0.1 \mu\text{m}$  gives a thickness of  $102 \mu\text{m}$ .

We have performed several measurements and the number of oscillations per spectral bandwidth is changing with time and varies between  $50 \mu\text{m}$  and  $200 \mu\text{m}$ , which is the order of size of the shim introduced between the two prisms. As a

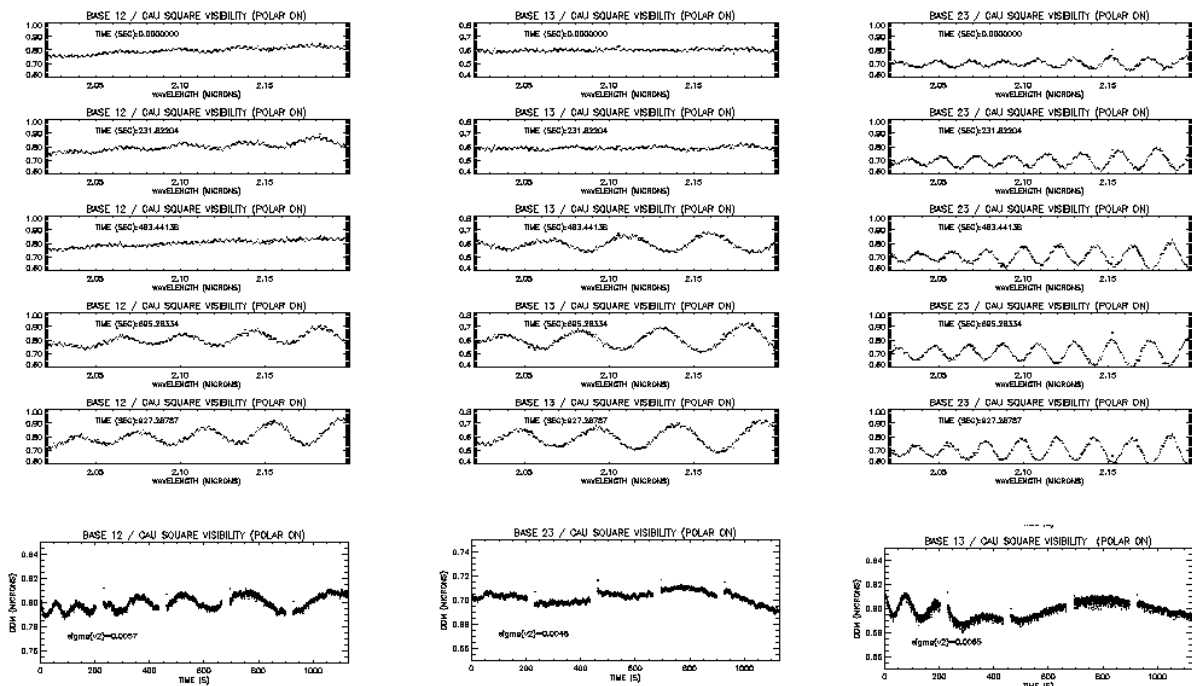


Figure 26: AMBER square visibilities recorded **with** the polarizers on the internal source. From left to right, the different baselines and from top to bottom a sequence of 5 consecutive exposures of 1000 frames lasting each about 50 seconds and separated by 20 seconds. These exposures have been averaged over the length of the exposure. Bottom panels represent the same time series with exposures averaged in wavelength but not in time.

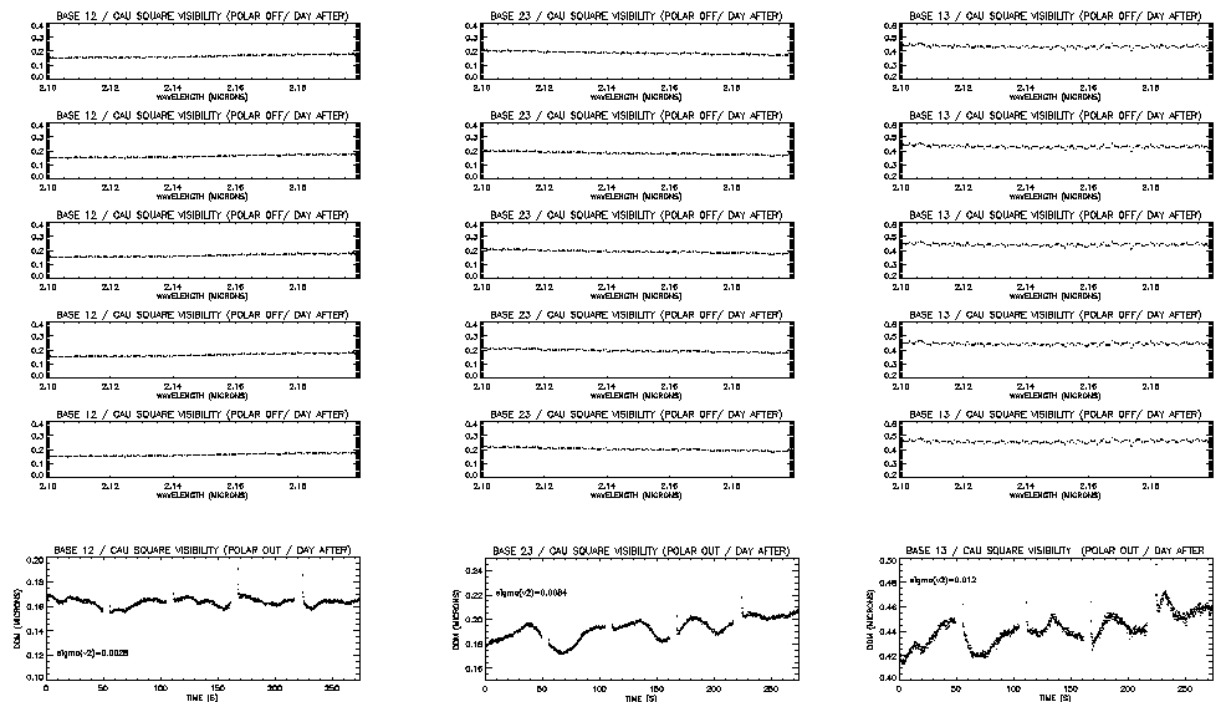


Figure 27: AMBER square visibilities recorded **without** the polarizers on the internal source. Same description as in Fig. 26. Note that the wavelength modulation has disappeared. The visibility fluctuation with time remains large, but may come also partly from a mechanical instability of an element of the internal source.

OCA/UNSA LAOG MPIfR/OAA	VLT / AMBER	Doc. No VLT-TRE-AMB-15830-7120
	February 2008 ATF run report <sup>1</sup>	Issue : 1.2 Date : 16/04/2008
		Page : 41 / 51

matter of fact, each baseline sees two polarizers and the interferences can create beating effects with a large range of frequency and amplitude.

The fact that the oscillations disappear when the polarizers are taken out is the final proof that these effects comes from the air blade present in the polarizers.

### G.3 Where to put the new polarizers?

Polarizers are however necessary to control the polarization. We have dismantled POL3 to try to place it in other part of the instrument. When putting it near the periscope in a place where the beam propagation was collimated, we obtained contrast of 0.9, 0.9 and 0.85 instead of 0.4, 0.6, 0.4. Therefore one should modify the instrument to introduce polarizers without air blades. Unless we succeed in understanding why the visibility drops to such low value without polarizers.

The present location of the polarizers is represented on Fig. 28. The location of the new polarizer should be chosen with great care. On the same figure, we propose two different locations. However, the position of one unique and common polarizer in the periscope tower should be privileged rather than 9 independant polarizers located at the output of the fibers.

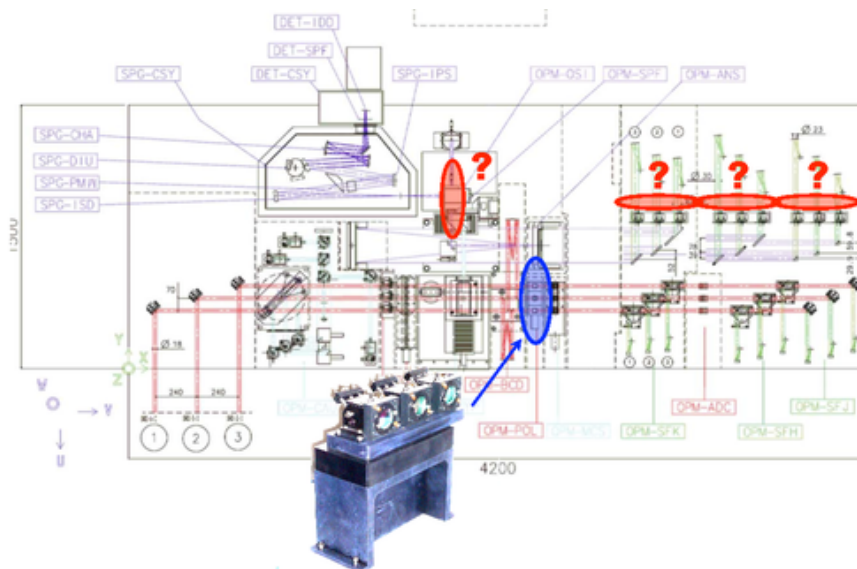


Figure 28: Location of the polarizers on the AMBER table (blue). Red ellipses show the possible locations for new polarizers. The position of one unique and common polarizer in the periscope tower (upper left) should be privileged.

## H Fabry-Pérot interferometer principle

[From Wikipedia, the free encyclopedia (<http://en.wikipedia.org/wiki/Fabry-Perot>)]

In optics, a Fabry-Pérot interferometer is typically made of a transparent plate with two reflecting surfaces, or two parallel highly reflecting mirrors. Its transmission spectrum as a function of wavelength exhibits peaks of large transmission corresponding to resonances of the etalon.

The resonance effect of the Fabry-Pérot interferometer is identical to that used in a dichroic filter. That is, dichroic filters are very thin sequential arrays of Fabry-Pérot interferometers, and are therefore characterised and designed using the same mathematics.

The varying transmission function of the FP is caused by interference between the multiple reflections of light between the two reflecting surfaces. Constructive interference occurs if the transmitted beams are in phase, and this corresponds to a high-transmission peak of the etalon. If the transmitted beams are out-of-phase, destructive interference occurs and this corresponds to a transmission minimum. Whether the multiply-reflected beams are in-phase or not depends on the wavelength ( $\lambda$ ) of the light (in vacuum), the angle the light travels through the FP ( $\theta$ ), the thickness of the etalon ( $l$ ) and the refractive index of the material between the reflecting surfaces ( $n$ ).

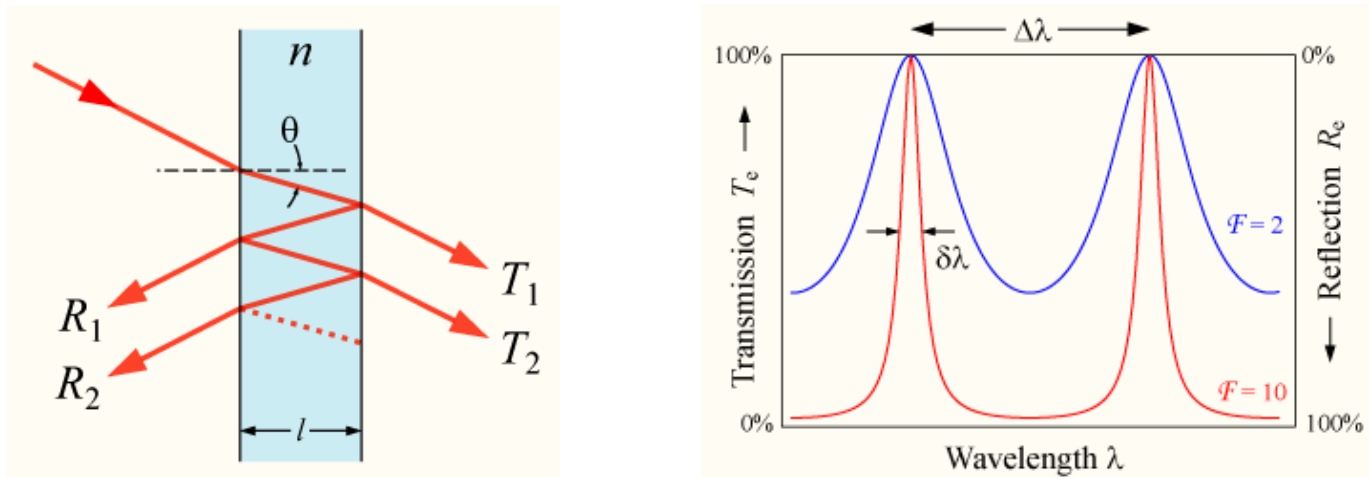


Figure 29: Left: A Fabry-Pérot interferometer. Light enters the etalon and undergoes multiple internal reflections. Right: The transmission of an etalon as a function of wavelength. A high-finesse etalon (red line) shows sharper peaks and lower transmission minima than a low-finesse etalon (blue).

The wavelength separation between adjacent transmission peaks is called the free spectral range of the FP,  $\Delta\lambda$ , and is given by:

$$\Delta\lambda = \frac{\lambda_0^2}{2nl \cos \theta + \lambda_0} \approx \frac{\lambda_0^2}{2nl \cos \theta} \quad (1)$$

where  $\lambda_0$  is the central wavelength of the nearest transmission peak.

Therefore the thickness of the étalon is given by:

$$l \approx \frac{\lambda_0^2}{2n \Delta\lambda \cos \theta} \quad (2)$$

## I Piezos controlling differential OPDs

During the ATF investigation, we were interested to know if the piezos which drives the fiber injection to control the differential OPDs could be at the origin of vibrations that could lead to visibility fluctuations. We have therefore taken exposures with the piezos on and off (see Figs. 30 and 31). This experience was made with the polarizers still on the table.

We have not detected any changes in the behavior of the visibility. When the piezos are off then all piezos move by 40 microns at the beginning of the stroke. We had to compensate these OPDs manually with the translation stage of the input dichroics which are known to unstable. Therefore the increase of the OPD changes seen on the right part of Fig. 31 are probably relaxation of these translation stages.

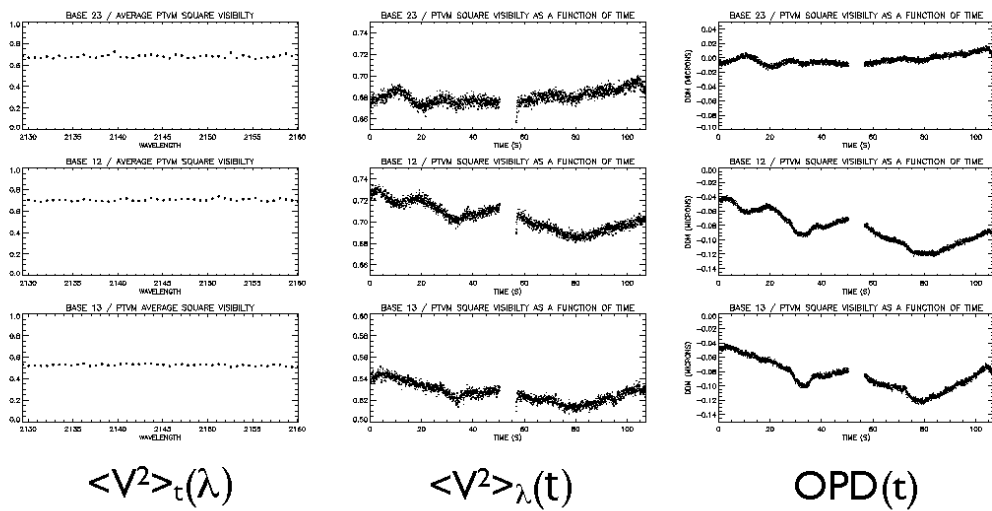


Figure 30: Square visibilities observed on the AMBER internal source with the **piezos activated** averaged in time plotted in function of wavelength (left), averaged in wavelength and plotted in function of time (middle) and the piston in function of time for the three baselines (from top to bottom).

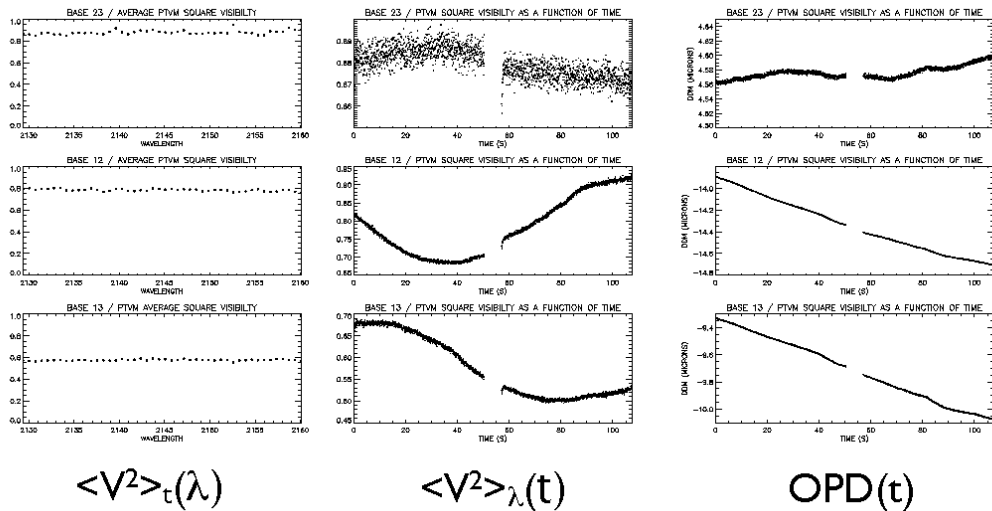


Figure 31: Square visibilities observed on the AMBER internal source with the **piezos deactivated**. The lay-out is the same as the one of Fig. 30.



## J Influence of injection into the fibers

We took the opportunity of the new piezo-controlled 'IRIS Fast Guiding' (IFG) positioning of the AMBER entrance beams and the availability of the AT beacons to test whether the injection of the beam creates or augments the "phase beating" effect (see sect. 4.2).

We found (see Fig. 32) that there is no effect detectable of the changes of injection (up to five core diameters) when the polarizer (Appendix G) is removed. The dispersed spectra of the beacons are devoid of amplitude structures (phase was not measurable since beacons are not one coherent source), and the flux injected simply diminishes as the injection worsens. In the presence of the polarisers, however, amplitude effects are present and vary in shape with the injection. That the small changes in the positioning of the beams induced by the IFG would produce this effect demonstrates how sensitive the experiment was to the differential Fabry-Pérot effect induced by the polarizer.

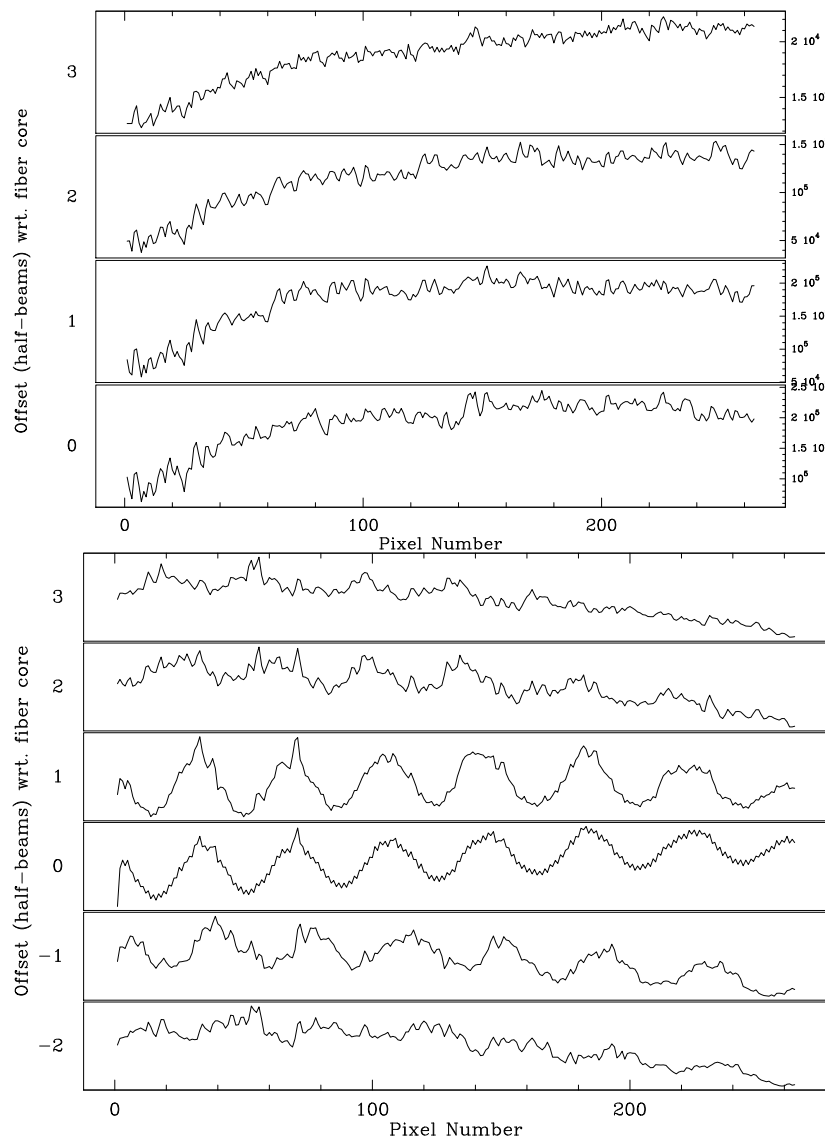


Figure 32: Flux recorded in one fiber with one AT beacon in function of the injection with (top) and without the polarizers (bottom). Injection condition were changed without touching AMBER but using the AMBER fast guiding piezos and moving by half an Airy disk.

OCA/UNSA LAOG MPIfR/OAA	VLT / AMBER	Doc. No VLT-TRE-AMB-15830-7120
	February 2008 ATF run report <sup>1</sup>	Issue : 1.2 Date : 16/04/2008 Page : 45 / 51

## K Observing calibrators without polarizers

The last night of ATF run was focused on the observations of 2 calibrators without FINITO in order to characterize AMBER without the polarizers:

- SAO 199118: diameter of  $2.54 \pm 0.037$  mas (Bordé), spectral type K2.5 II-III and
- SAO 249932: diameter of  $2.19 \pm 0.053$  mas (Bordé), spectral type K5 III,

and a larger star SAO 218755. We have reduced these data in order to display the curve of the transfer function (see Fig. 34). We have also computed the differential phase and the closure phase.

The result of this night is:

- transfer function (see Fig. 34): accuracy of the order of the percent. However it changes with seeing conditions and coherence time and therefore calibrations should be done as close as possible from the target science.
- Differential phase (see Fig. 35) are zero at veru good accuracy (less than  $10^{-2}$  rad, i.e. within specifications).
- Closure phases (see Fig. 36) are not very accurate on this sample night. A reason might be that the SNR depends on the value of the visibilities which were small for two baselines due to the absence of polarizers (see values in Fig. 34).

During this night, we have interlaced the observation of the star SAO 218755 which has an expected diameter of 6.4mas. Interestingly, the longest baseline crosses the first lobe and therefore we were able to see a  $\pi$  shift in the closure phase validating the closure phase measurement (see Fig. 33)

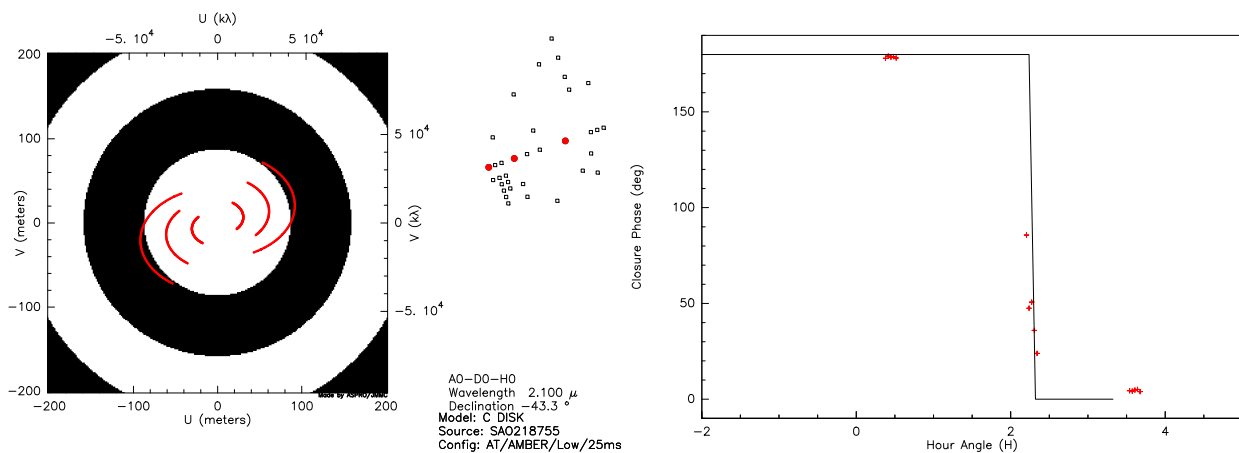


Figure 33: Closure phase measured on the star SAO 218755. Left: uv coverage overplot on the closure phase change due to the diameter. Right: measured closure phase (red crosses) with the expected closure phase change (solid black line).

Observations performed on 2008-02-14

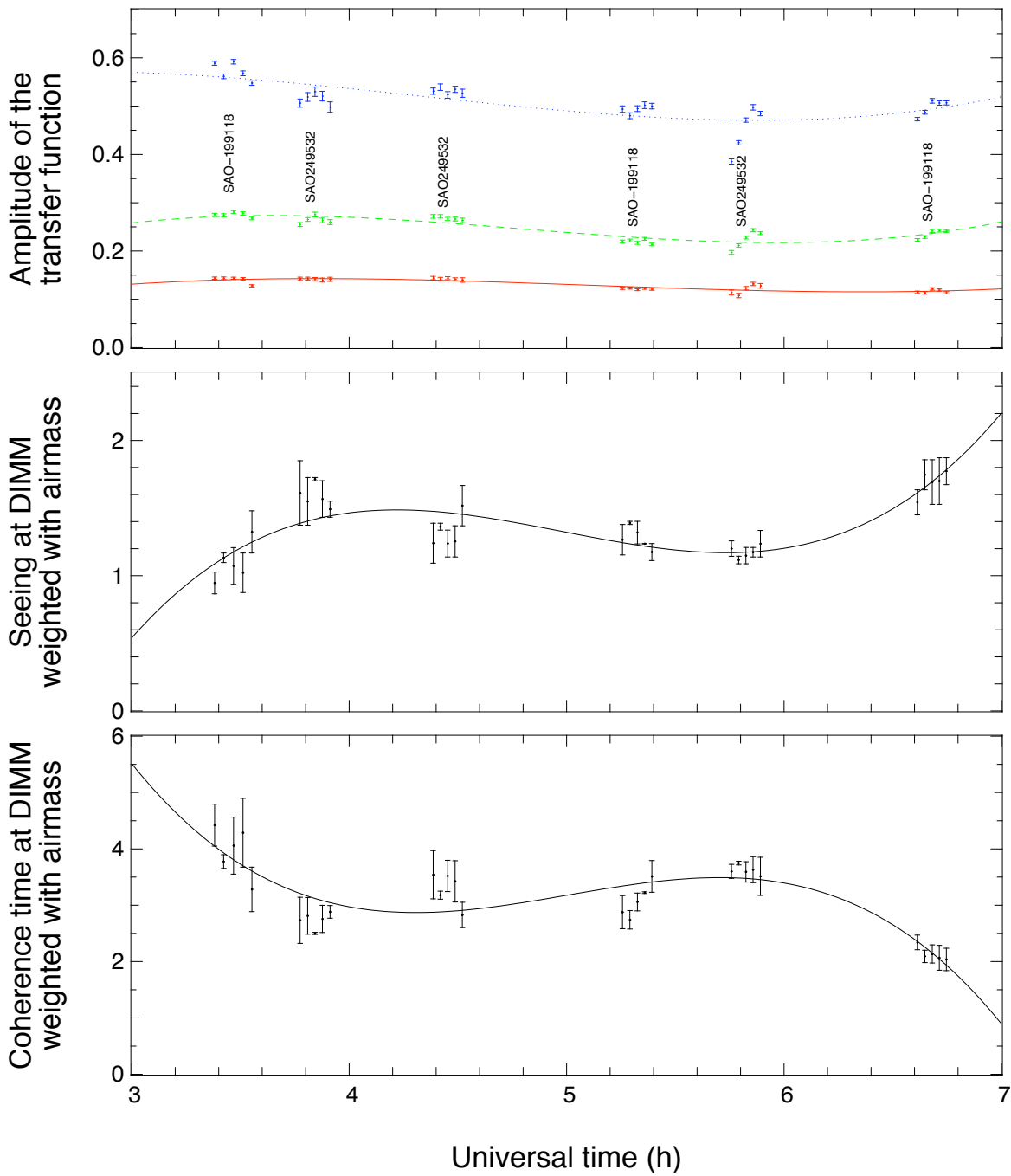


Figure 34: Variations of the transfer function averaged over the wavelength for the two calibrators SAO 199118 and SAO 249932 observed over 4 hours in MR, without FINITO and without the polarizer.

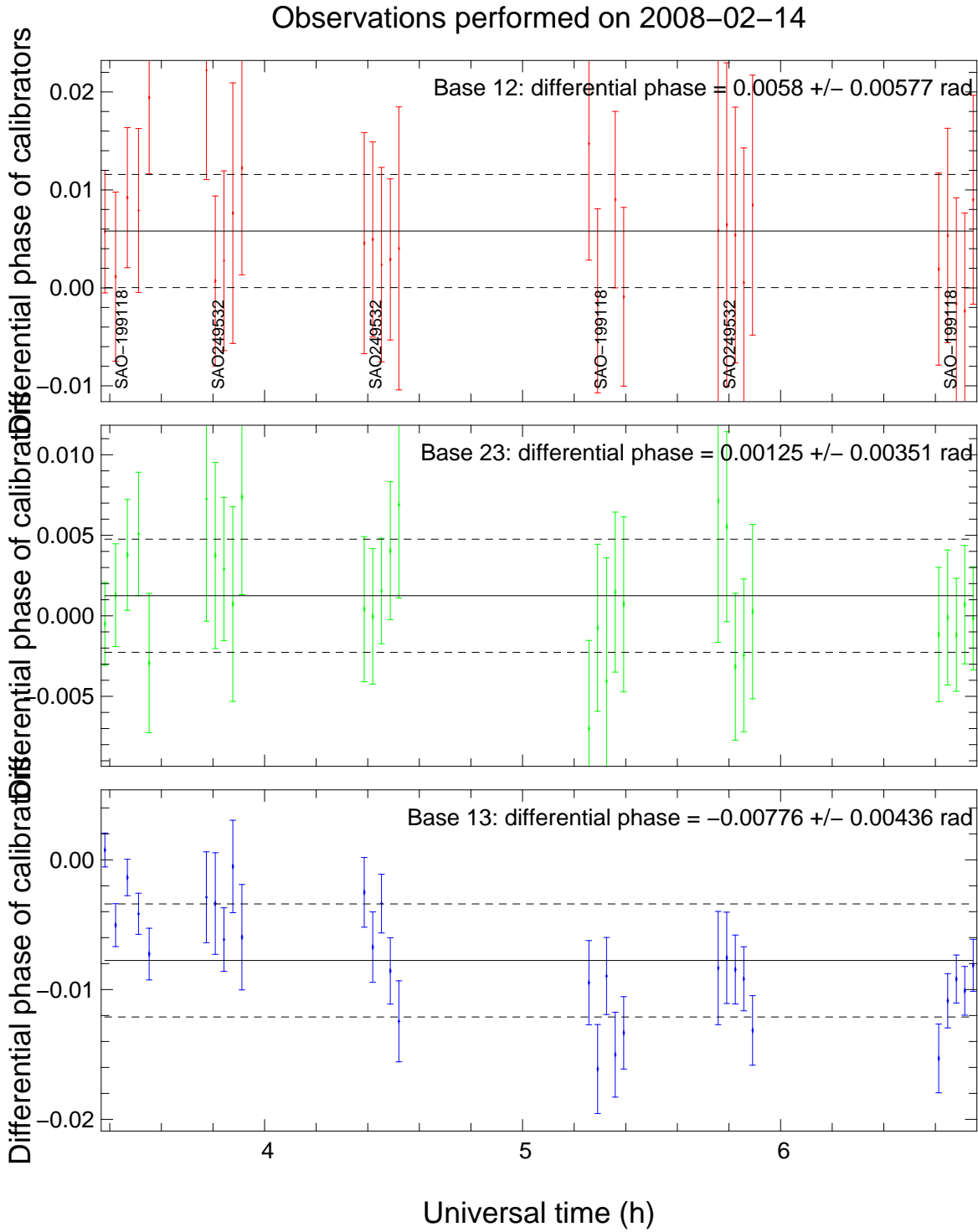


Figure 35: Variations of the differential phases averaged over the wavelength for the two calibrators SAO 199118 and SAO 249532 observed over 4 hours in MR, without FINITO and without the polarizer.

Observations performed on 2008-02-14

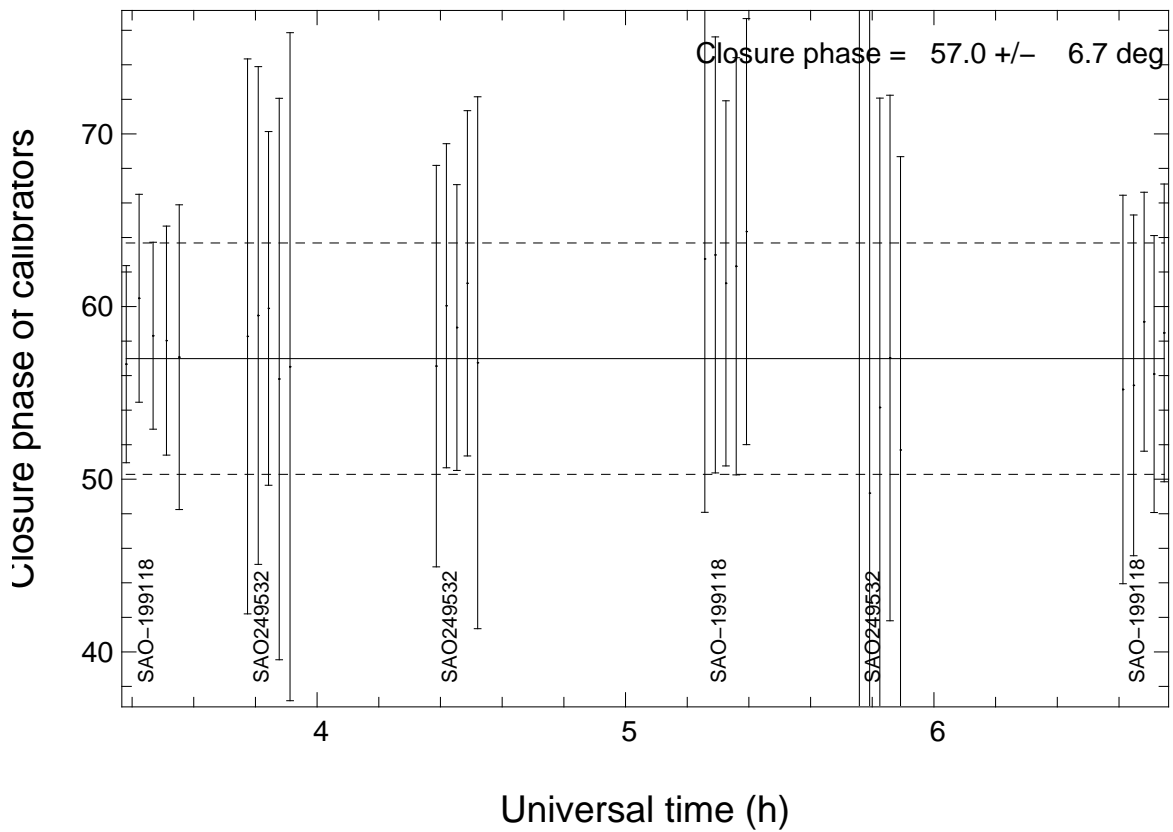


Figure 36: Variations of the closure phase averaged over the wavelength for the two calibrators SAO 199118 and SAO 249932 observed over 4 hours in MR, without FINITO and whithout the polarizer.

Table 4: AMBER performance on calibrators without the polarizers.

SAO Number	Time (hours)	$V_{12}^2$	$\sigma(V_{23}^2)$	$V_{13}^2$	$\sigma(V_{12}^2)$	$V_{23}^2$	$\sigma(V_{13}^2)$	$\phi_{12}$	$\phi_{23}$ (degrees)	$\phi_{13}$	$\psi_{123}$ (degrees)
199118	0.00	0.156	0.003	0.067	0.005	0.012	0.004	0.00	-0.002	-0.01	55.74
199118	0.04	0.141	0.004	0.065	0.005	0.011	0.005	0.01	-0.004	-0.02	59.51
199118	0.09	0.158	0.003	0.069	0.005	0.012	0.004	0.00	-0.018	0.00	57.16
199118	0.13	0.146	0.004	0.066	0.006	0.011	0.004	0.01	-0.007	-0.02	56.83
199118	0.17	0.135	0.004	0.060	0.007	0.008	0.006	0.02	-0.002	-0.07	55.90
249532	0.39	0.160	0.012	0.062	0.009	0.017	0.007	0.01	-0.040	-0.01	55.64
249532	0.43	0.168	0.012	0.067	0.009	0.017	0.007	0.01	-0.008	-0.11	58.07
249532	0.46	0.176	0.012	0.072	0.009	0.016	0.006	0.02	-0.007	0.04	57.67
249532	0.50	0.170	0.013	0.066	0.011	0.016	0.008	0.01	-0.022	-0.06	54.96
249532	0.53	0.155	0.013	0.064	0.011	0.016	0.009	0.02	-0.019	-0.09	56.95
249532	1.01	0.180	0.009	0.070	0.007	0.017	0.008	0.01	0.010	0.10	57.18
249532	1.04	0.186	0.008	0.070	0.006	0.017	0.007	0.02	0.004	0.10	59.50
249532	1.07	0.175	0.008	0.068	0.006	0.017	0.006	0.01	0.007	0.07	58.33
249532	1.11	0.183	0.008	0.068	0.006	0.016	0.006	0.03	-0.009	0.04	60.60
199118	1.88	0.127	0.008	0.045	0.006	0.012	0.005	0.05	0.021	-0.04	61.20
199118	1.91	0.122	0.008	0.045	0.006	0.012	0.004	0.08	-0.002	0.01	60.82
199118	1.94	0.157	0.008	0.082	0.006	0.038	0.004	0.05	-0.140	-5.08	57.71
199118	1.98	0.134	0.008	0.047	0.006	0.012	0.004	0.06	-0.007	0.01	61.99
199118	2.01	0.133	0.007	0.042	0.005	0.012	0.004	0.06	0.006	-0.02	62.30
249532	1.14	0.178	0.011	0.066	0.009	0.016	0.010	0.04	0.027	0.09	55.29
249532	2.38	0.100	0.008	0.037	0.009	0.011	0.012	0.04	0.009	-0.07	26.20
249532	2.41	0.121	0.007	0.043	0.007	0.010	0.010	0.05	-0.059	0.19	46.11
249532	2.44	0.149	0.006	0.050	0.006	0.013	0.008	0.04	-0.004	0.09	52.37
249532	2.48	0.167	0.007	0.057	0.006	0.015	0.008	0.03	-0.001	-0.05	54.33
249532	2.51	0.158	0.007	0.054	0.006	0.014	0.010	0.06	-0.015	0.01	51.49
199118	3.23	0.146	0.005	0.047	0.005	0.011	0.005	0.05	0.010	-0.06	54.59
199118	3.27	0.156	0.005	0.050	0.005	0.011	0.005	0.05	-0.012	0.02	55.35
199118	3.30	0.173	0.005	0.055	0.004	0.013	0.005	0.04	0.020	0.09	57.73
199118	3.33	0.170	0.005	0.055	0.004	0.012	0.005	0.04	-0.007	-0.02	56.69
199118	3.37	0.171	0.004	0.055	0.004	0.011	0.005	0.03	-0.014	-0.01	57.66

OCA/UNSA LAOG MPIfR/OAA	VLT / AMBER	Doc. No VLT-TRE-AMB-15830-7120
	February 2008 ATF run report <sup>1</sup>	Issue : 1.2
		Date : 16/04/2008
		Page : 50 / 51

## L Log book of the ATF run

- \* 31-Jan to 5-Feb:
  - o pupil alignment
  - o OPD de-saturation
- \* 6 Feb:
  - o H-band pupil alignment + OPD de-saturation
  - o ghost characterization
  - o overall stability control
- \* 7-Feb:
  - o find the fringe beating, characterize it at LR, MR and HR
  - o Tests: crossing fibers. No improvement. Crossing does not change injection significantly, but adds a 7.5mm piston. Fringes still visible i HR. No significant improvement on phase beating.
  - o remove the polarizers and test at LR, MR and HR: no more fringe beating (but lower --by half-- fringe contrast).
    - + flux in K much higher and spectrum very different
    - + still a phase closure on the CAU of 6°
    - + We realize that by shutting down the RAS JH fiber, the K spectrum becomes very different --> strong K pollution through the JH fiber.
    - + Additionnally, now, the RAS light gives a closure of 0° !
  - o tests on sky on Sirius in MR and HR with 2 telescopes
- \* 8-Feb:
  - o discussion with RPe on status
  - o discussion with Pedro on alignment procedures
  - o test of a single fibered source in RAS: strongly reduced flux beating
  - o put POL3 after output f fibers close to the periscope in // beams: higher contrast: 0.9 0.9 0.85
  - o discussion with Andres on software procedures.
  - o try some Sirius 3T obs with this setup
- \* 9-Feb
  - o put back the POL3 at its 'nominal' position
  - o AMBER is fully realigned
  - o test of an Ocean Optics source in entrance of the fiber K: flux in J and H is higher than with normal RAS lamp but there is absorption due to dichroics.
  - o tests of piezos: 10mV noise corresponding to 0.1 microns amplitude
  - o Observations on CAU show OPD drifts and visibility fluctuations.
  - o laser for spectral calibration: PKe explains to FMa how it works.
  - o test on switched-off piezo: it seems that visibilities are higher with piezo off than on, but we still see changes of several % in minutes.
- \* 10-Feb
  - o test of the stability of the output beams in 0th-order and also in MR-K: conclusion, this is not the reason for the visibility fluctuations.
  - o fibers to be inverted: not possible in LR and MR because the OPD difference is about 7mm.
  - o test with the BCD to identify if the source of fluctuations is before or after the BCD: BCD in & out with piezos off in MR.
  - o OPD on or off to see differences
  - o bang tests in H and K.
  - o foreseen: test switching off all motors. Piezos have been shut down.

OCA/UNSA LAOG MPIfR/OAA	VLT / AMBER	Doc. No VLT-TRE-AMB-15830-7120
	February 2008 ATF run report <sup>1</sup>	Issue : 1.2
		Date : 16/04/2008
		Page : 51 / 51

\* 11-Feb

- o different DIT in MR to see the origin of vibrations if any...: no dependance
- o different DIT in H & K LR to see the origin of vibrations if any: no dependance -> is there really vibrations?
- o check the CAU source: PKe's source enlight K, H & J but presence of absorption line due to dichroics
- o display the K-LR fringes on RTD and locate sensitive optical parts: the large parabola of CAU is very sensitive
- o P2VM? + obs. in LR with no piezo to check that the variation of  $V^2$  come or not from piezzos: impossible to do because of OS software limitations. P2VM? requires piezo on for 1/4 dephasing and the software forces them to be at 40um. No piezos means an OPD of 40um... We stopped.
- o P2VM? + obs. in MR: OK but we have still fluctuations: does it mean that piezos are out of questions?
- o Observation with the beacons for bias estimation
- o Scan of the fiber inputs with the beacon to see influence of incidence (polarizer on)
- o Polarizer is taken out: no more photometry socks
- o Data reduction of previous data: the fluctuations are large, changing in wavelength, in amplitude,...: This is probably teh origin of  $V^2$  fluctuations.
- o Record of data without polarizers for comparison: V12 and V23 are about 0.4 when V23 is about 0.8 without polarizers. Still fluctuations.

\* 12-Feb

- o New measurements in MR-K: the data is much more stable
- o meeting and visit of the lab with P. Haguenaer
- o discussion with JBLB
- o experiment with perturbation of the large parabola in the CAU
- o telecon with R. Petrov
- o On sky measurements in MR-K: bright, medium and faint stars. Measurements with and w/o FINITO with DIT from 25ms to 200ms
- o level of fluxes in K (H and J not realigned after the POL removed): gain between 500% and 700% without the POL.
- o adjustment of LR-H for observations in LR-JHK (J needs to be adjusted)
- o observations in LR-JHK with FINITO.

\* 13-Feb

- o Discussion on the objective of the night: focused on MR-K
- o readjustment of H and J + OPD
- o beampos (careful with RAS)
- o LR- spectral calibration: script edition
- o start preset the telescopes at 22:30
- o observe all night in MR-K without polarizers on calibrator stars

\* 14-Feb

- o put back the polarizers
- o check the optical alignment in all bands
- o perform the spectral calibration with piezo scan (give also loss of coherence in LR)